Eddy-driven sources and sinks of nutrients in the upper ocean: Results from a 0.1° resolution model of the North Atlantic

D. J. McGillicuddy Jr. and L. A. Anderson

Department of Applied Ocean Physics and Engineering, Woods Hole Oceanographic Institution, Woods Hole, Massachusetts, USA

S. C. Doney

Department of Marine Chemistry and Geochemistry, Woods Hole Oceanographic Institution, Woods Hole, Massachusetts, USA

M. E. Maltrud

Theoretical Fluid Dynamics, Los Alamos National Laboratory, Los Alamos, New Mexico, USA

Received 18 September 2002; revised 15 November 2002; accepted 21 November 2002; published 11 April 2003.

[1] A nitrate-based model of new production is incorporated into eddy-resolving (0.1°) simulations of the North Atlantic. The biological model consists of light and nutrient limited production within the euphotic zone and relaxation of the nitrate field to climatology below. Sensitivity of the solutions to the parameters of the biological model is assessed in a series of simulations. Model skill is quantitatively evaluated with observations using an objective error metric; simulated new production falls within the range of observed values at several sites throughout the basin. Results from the "best fit" model are diagnosed in detail. Mean and eddying components of the nutrient fluxes are separated via Reynolds decomposition. In the subtropical gyre, eddy-driven vertical advection of nutrients is sufficient to overcome the mean wind-driven downwelling in the region and fuels a significant fraction of the annual new production in that area. In contrast, eddies constitute a net sink of nutrients in the subpolar gyre. Geostrophic adjustment to deep winter convection through mesoscale processes causes a net flux of nutrients out of the euphotic zone; the magnitude of this sink is sufficient to counterbalance the mean wind-driven upwelling of nutrients over much of the region. On the basis of these simulations it appears that the oceanic mesoscale has major impacts on nutrient supply to, and removal from, the euphotic zone. *INDEX TERMS:* 4255 Oceanography: General: Numerical modeling; 4520 Oceanography: Physical: Eddies and mesoscale processes; 4572 Oceanography: Physical: Upper ocean processes; 4805 Oceanography: Biological and Chemical: Biogeochemical cycles (1615); 4845 Oceanography: Biological and Chemical: Nutrients and nutrient cycling; *KEYWORDS:* new production, mesoscale processes, eddies, biogeochemical cycling, physical-biological interactions

Citation: McGillicuddy, D. J., Jr., L. A. Anderson, S. C. Doney, and M. E. Maltrud, Eddy-driven sources and sinks of nutrients in the upper ocean: Results from a 0.1° resolution model of the North Atlantic, *Global Biogeochem. Cycles*, *17*(2), 1035, doi:10.1029/2002GB001987, 2003.

1. Introduction

[2] The fact that geochemical estimates of new production in the oligotrophic waters of the open ocean far surpass that which can be sustained by traditional mechanisms of nutrient supply has been problematic for some time [*Schulenberger and Reid*, 1981; *Jenkins*, 1982; *Jenkins and Goldman*, 1985]. Three independent transient tracer techniques all indicate that new production in the Sargasso Sea is of the order of 0.5 mol N m^{-2} yr^{-1}: oxygen production in the euphotic zone [*Jenkins and Goldman*, 1985; *Spitzer and Jenkins*, 1989], oxygen consumption in the aphotic zone [*Jenkins and Goldman*, 1985; *Sarmiento et al.*, 1990; *Jenkins and Wallace*, 1992], and the He flux gauge [*Jenkins*, 1988a]. Approximately one quarter to one third of the annual nutrient requirement can be supplied by entrainment into the surface mixed layer, caused by wintertime convection [*Michaels et al.*, 1994]. Modern estimates of mixing rates in the thermocline [*Lewis et al.*, 1986; *Ledwell et al.*, 1993, 1998] combined with the observed nutrient gradient at the base of the euphotic zone suggest that diapycnal diffusion contributes very little. The mean wind-driven vertical motion in the main subtropical gyre is oriented

0886-6236/03/2002GB001987$12.00

downward due to the negative wind stress curl in the region and therefore represents a net sink, rather than a net source, of nutrients. The surface Ekman drift does advect nutrients horizontally toward the interior of the gyre, but recent calculations suggest that the net contribution of the total wind-driven transport is small and positive, at least for the inorganic species of nitrogen [*Williams and Follows*, 1998]. Together, these processes account for less than one half the annual new production. It has been suggested that nitrogen fixation could be responsible for the remainder of the phytoplankton nutritional requirement, yet rate estimates for this region vary by an order of magnitude [*Michaels et al.*, 1996; *Lipschultz and Owens*, 1996; *Capone et al.*, 1997; *Gruber and Sarmiento*, 1997; see also *Hood et al.*, 2000].

[3] The notion that mesoscale processes could be an important vehicle for nutrient transport in the world's oceans has been debated for many years [e.g., *Woods*, 1988; *Fasham et al.*, 1985; *Franks et al.*, 1986; *Falkowski et al.*, 1991; *Strass*, 1992; *Flierl and Davis*, 1993; *Dadou et al.*, 1996; *Smith et al.*, 1996; *Spall and Richards*, 2000; *Mahadevan and Archer*, 2000; *Garçon et al.*, 2001; *Martin et al.*, 2002]. Comparison of two hydrographic profiles sampled 1 month apart in summer 1986 off Bermuda documented an apparently eddy-driven nutrient injection event that could account for 20–30% of the annual new production [*Jenkins*, 1988b]. Since then, substantial evidence has accumulated which suggests that mesoscale eddies constitute a significant mode of nutrient transport in the Sargasso Sea [*McGillicuddy et al.*, 1998]. Regional numerical simulations suggest that eddy-induced upwelling causes intermittent fluxes of nitrate into the euphotic zone of magnitude sufficient to balance the nutrient demand implied by geochemical estimates of new production [*McGillicuddy and Robinson*, 1997]. Nitrate flux calculations, based on satellite altimetry and a statistical model linking sea level anomaly to subsurface isopycnal displacements, yield comparable estimates [*Siegel et al.*, 1999]. Observations of an eddy-driven nutrient pulse were obtained at the Bermuda Testbed Mooring [*McNeil et al.*, 1999]. Mesoscale biogeochemical surveys documented that eddy-induced upward displacement of density surfaces can inject nutrients into the euphotic zone, resulting in accumulation of phytoplankton biomass in the overlying waters [*McGillicuddy et al.*, 1999]. Similar patterns emerge from an analysis of satellite-derived sea surface temperature and pigment fields, with higher pigment biomass occurring in mesoscale features consisting of cold temperature anomalies and lower pigment biomass occurring in mesoscale features consisting of warm temperature anomalies [*McGillicuddy et al.*, 2001].

[4] Until recently, computational limitations precluded the treatment of mesoscale processes in basin-scale biogeochemical models. Generally speaking, the hydrodynamic foundations for such models fit into three loosely defined categories: coarse-resolution, eddy-permitting, and eddy-resolving. Experience has shown that grid spacing smaller than the Rossby radius of deformation is required for accurate representation of mesoscale phenomenology. This is an especially stringent requirement for basin-scale models as the Rossby radius varies as a function of latitude. Resolution of the order of 0.1° is necessary to satisfy this constraint throughout typical basin-wide domains [*Smith et al.*, 2000], yet some aspects of eddy-resolving simulations continue to improve as resolution is increased substantially beyond that value [e.g., *Hurlburt and Hogan*, 2000]. Coarse-resolution models, with grid spacing that is many multiples of the Rossby radius (order 1°), simply cannot admit mesoscale processes and therefore result in highly smoothed fields. Eddy-permitting models fall somewhere in between as mesoscale processes begin to emerge at resolutions of the order of 1/2°–1/6°. However, simulated eddy kinetic energies in eddy-permitting models are typically lower than observed, and certain aspects of the time-mean circulation are problematic [see *Smith et al.*, 2000, and references therein].

[5] The seminal work of *Sarmiento et al.* [1993] and *Fasham et al.* [1993] documented the first substantial effort to use a planktonic ecosystem model embedded in a general circulation model (GCM) to investigate the physical-biological interactions that impact biogeochemical budgets in the North Atlantic. Their general approach was to incorporate *Fasham et al.* 's [1990] seven-compartment nitrogen-based biological formulation into a relatively coarse-resolution (2°) primitive equation circulation model. Under seasonal climatological forcing conditions, the coupled model was run out to a quasi steady statistical equilibrium, and the underlying controls were diagnosed. Subsequent work has included a parameter dependence and sensitivity analysis of these numerical solutions conducted by *Slater et al.* [1993] and some initial experiments involving assimilation of satellite-derived chlorophyll distributions [*Armstrong et al.*, 1995]. *Oschlies and Garçon* [1998, 1999] and *Oschlies et al.* [2000] used a simpler four-compartment nutrient-phytoplankton-zooplankton-detritus (NPZD) ecosystem model in an eddy-permitting (1/3°) resolution model of the North Atlantic. *Dutkiewicz et al.* [2001] examine interannual variations in basin-scale chlorophyll patterns using a simple ecosystem model in a coarse-resolution GCM, while *Chu et al.* [2003] examine a more complex (10-component) ecosystem model in a global eddy-permitting GCM.

[6] Detailed comparisons of these simulations with observations have revealed mixed results. One aspect in which the model solutions agree with data is in the large-scale chlorophyll distribution [*Sarmiento et al.*, 1993; *Oschlies et al.*, 2000]. The overall pattern in the annual mean concentration is similar to satellite-based estimates from the Coastal Zone Color Scanner, including low pigment in the main subtropical gyres and higher concentrations in upwelling regions and the subpolar gyre. Furthermore, the modeled seasonal variations about the annual mean also compare favorably with observations. Given the fact that such simulations were constructed using a fixed set of ecosystem parameters over the entire domain, this agreement is especially intriguing.

[7] Although such models capture the general characteristics of the seasonal changes in surface chlorophyll, comparison with time series data at fixed points reveals significant discrepancies. For example, wintertime nitrate concentrations at station S exceed observed values by up to

Table 1. Nitrate Budgets and Annual New Production at the BATS Site in Three Different Models[a]

	Fasham et al. [1993], 2.0° (Coarse-Resolution)	*Oschlies et al.* [2000], 0.3° (Eddy-Permitting)	This Study, 0.1° (Eddy-Resolving)[b]
Horizontal transport	0.38	0.10	0.04 ± 0.01
Vertical advection	−0.16	−0.13	0.12 ± 0.01
Vertical mixing[c]	0.35	0.66	0.47 ± 0.04
Convection	0.34		0.37 ± 0.03
Diffusion	0.01		0.10 ± 0.01
Annual new production	0.57	0.64–0.69	0.63 ± 0.04

[a]Nitrate budgets and annual new production are in mol N m^{-2} yr^{-1}. Geochemical estimates in this region suggest an annual new production of 0.50 ± 0.14 mol N m^{-2} yr^{-1} (Table 5).

[b]Solutions were smoothed with a 24-point *e*-folding Gaussian filter prior to extraction of these point-wise results.

[c]Vertical mixing is the sum of convection and diffusion. *Oschlies et al.* [2000] do not distinguish between convection and diffusion in the vertical mixing term.

an order of magnitude [*Fasham et al.*, 1993; *Oschlies et al.*, 2000]. The vertical structure of the simulated distribution is also problematic in that the nitracline is much shallower and sharper than is observed. Simulated phytoplankton concentration and primary production tend to have seasonal cycles of much higher amplitude than what is observed. These systematic errors tend to compensate for each other in terms of annual primary production: A mean value in accordance with observations is produced by overestimation during the bloom period and by underestimation during the oligotrophic period.

[8] Annual average term balances near Bermuda (Table 1) permit quantification of the transport pathways, through which nutrients are supplied to sustain the simulated productivity. In the *Fasham et al.* [1993] analysis, nitrate supply is dominated by horizontal advection, mostly in the meridional direction. Convection is the next largest contribution to the annual budget, but nearly one half of the convective input is counterbalanced by downwelling driven by Ekman convergence (the vertical advection term). Diffusion plays only a minor role, and the balance of terms yields an annual new production that is within the range of geochemical estimates (0.50 ± 0.14 mol N m^{-2} yr^{-1}). In contrast, the eddy-permitting simulation of *Oschlies et al.* [2000] suggests far less lateral input of nitrate in this region. The annual new production of 0.64–0.69 mol N m^{-2} yr^{-1} is at the upper limit of observational estimates and is almost entirely driven by vertical mixing (*Oschlies et al.* [2000] do not distinguish between convection and diffusion in their model). Interestingly, both the coarse-resolution and eddy-permitting simulations predict similar fluxes due to vertical advection (net transport out of the euphotic zone). Both are forced with monthly climatological winds described by *Hellerman and Rosenstein* [1983], so the Ekman downwelling driven by wind stress curl is likely comparable in the two models. If the bulk fluxes of nitrate are not sensitive to differences in either (1) the biogeochemical models or (2) the simulated nitrate fields on which the transport processes operate, it could be inferred that eddy activity in the *Oschlies et al.* [2000] eddy-permitting model does not contribute significantly to new production near Bermuda. Here we present high-resolution (0.1°) eddy-resolving simulations of the North Atlantic which suggest that vertical transport associated with mesoscale features is sufficiently strong to overcome Ekman downwelling in the subtropical gyre, causing vertical advection to be a net source of nitrate in this region. Quite unexpectedly, the model results also indicate that eddy-driven fluxes cause a net sink of nitrate in the subpolar gyre. This sink appears to result from the impact of mesoscale processes on restratification following wintertime deep convection.

2. Methods

2.1. Physical Model

[9] The coupled physical-biogeochemical model is based on the Los Alamos Parallel Ocean Program [*Smith et al.*, 1992]. It is a level coordinate model that solves the three-dimensional primitive equations with a free surface and realistic bottom topography. Essentially, it is an implementation of primitive equation ocean dynamics described by *Bryan* [1969], with a number of important numerical improvements. In addition, it has been adapted to run efficiently on massively parallel computational architectures.

[10] The model domain extends from 20°S in the South Atlantic to 72.6°N in the North Atlantic and from 98°W to 17.2°E. It includes the Gulf of Mexico and the western Mediterranean Sea but excludes Hudson Bay. The computational mesh consists of a Mercator grid with a resolution of $\Delta\lambda = 0.1°$ and $\Delta\phi = 0.1° \cos\phi$, where λ and ϕ are longitude and latitude, respectively. The horizontal resolution varies from 11.1 km at the equator to 3.2 km at the northern boundary, such that the grid spacing is everywhere less than or equal to the zonal mean Rossby radius of deformation. The vertical grid consists of 40 nonuniformly spaced levels, distributed in a Gaussian function of depth. Level thicknesses vary from ~10 m at the surface to 250 m below 3500 m. Bathymetry is derived from the 1/12° resolution ETOPO5 database from the National Geophysical Data Center.

[11] Subgrid-scale horizontal mixing processes are parameterized with a biharmonic operator. Viscosity and diffusivity vary with the cube of the grid spacing, with values at the equator of 2.7×10^{10} and 0.9×10^{10} m^4 s^{-1}, respectively. Vertical viscosities and diffusivities are computed based on the Richardson number formulation described by *Pacanowski and Philander* [1981], with background values of 10^{-4} and 10^{-5} m^2 s^{-1}, respectively. In addition to this explicit integration of the vertical mixing terms, two passes of a standard convective adjustment scheme are made each time step. A quadratic bottom stress is applied at the ocean bottom.

[12] The model ocean is initialized at rest, with temperature and salinity values set to their climatological values for June in the *Levitus* [1982] climatology. Surface forcing

Table 2. Parameters of the Nutrient Transport Model

Parameter	Value
Maximum new production rate μ_0, mmol N m^{-3} d^{-1}	0.25–0.5
Half saturation constant for nitrate limitation k_n, mmol N m^{-3}	0.1
Initial slope of light response α, m^2 W^{-1}	0.05
Nitrate-restoring timescale τ, days	10–60

consists of 6-hour European Centre for Medium-Range Weather Forecasts (ECMWF) surface wind analyses averaged over daily intervals, with surface heat fluxes derived from the *Barnier et al.* [1995] monthly climatology. Freshwater fluxes are simulated by restoring surface salinity to daily interpolations of the *Levitus* [1982] monthly climatology. There are 3°-wide buffer zones at the northern, eastern, and southern boundaries, in which temperature and salinity are also restored to the Levitus climatology throughout the water column; the restoring timescale varies linearly from 0 days at the boundary to 15 days at the edge of the buffer.

[13] The physical model is spun-up for a period of 11.5 years, using repeating winds from 1985 to 1991. During this time the model reaches a state of quasi-equilibrium. Kinetic energy reaches stationarity in 2–3 years, which is a typical timescale for baroclinic adjustment of the velocity field to an initial density distribution. Volume-averaged temperature approaches a steady annual cycle after ~10 years. Although these integrated statistics suggest that the initial phase of rapid adjustment to initial conditions is complete, there is a much longer timescale (of the order of the turnover time for the entire basin) for the model to achieve true equilibrium. Current computational capabilities do not permit routine integrations of such duration. However, full equilibrium is not required for the present study.

[14] See *Smith et al.* [2000] for a detailed description of the 0.1° simulation, on which the coupled model is based. Note that in this context the coupling of the models is one-way; that is, the physics influences the biogeochemistry, but there is no biogeochemical feedback to the physics.

2.2. An Idealized Nutrient Transport Model

[15] In order to ascertain the impact of various circulation processes on nutrient transport to the upper ocean, an idealized one-tracer model representing nitrate was incorporated into the physical model described in section 2.1. In this model the water column is partitioned into a euphotic zone (above 104 m), where biological uptake of nitrate occurs, and an aphotic zone (below 104 m), where nitrate is restored to its observed concentration as a spatial function of density via a first-order process. Nitrate uptake by phytoplankton is assumed to take the form

$$\text{uptake rate} = \mu \min(Q, L),$$

where the temperature-dependent maximal uptake rate μ (mmol N m^{-3} d^{-1}) is modulated by nondimensional light and nutrient limitation factors via Liebig's Law of the Minimum [*Browne*, 1942; *Ondercin et al.*, 1995; *Hurtt and Armstrong*, 1996]. Note that the uptake rate μ used here is an absolute rate rather than the specific rate commonly used in ecosystem models that explicitly resolve fluctuations in biomass. Nutrient limitation Q is expressed in Michaelis-Menten form, whereas light limitation L is formulated as an exponential function characteristic of traditional photosynthesis versus irradiance relationships [e.g., *Platt et al.*, 1980], although effects of photoinhibition are neglected:

$$Q = N/(k_n + N)$$

$$L = 1 - \exp(-\alpha I),$$

where N is nitrate concentration, k_n is the half-saturation constant for nitrate uptake, α is the initial slope of the photosynthesis versus irradiance relationship, and I is the photosynthetically available radiation. The temperature dependence of the maximal rate is given by *Eppley*'s [1972] formula $\mu = \mu_0\ 1.884^{(T-20)/10}$. Photosynthetically available radiation I is assumed to be 45% of the shortwave flux specified in the *Barnier et al.* [1995] monthly climatology. A constant extinction coefficient of 0.044 m^{-1} is used to compute the underwater light field. The impact of mixing on new production in the surface layer is modeled by subjecting the entire mixed layer to a light intensity that is averaged over that depth interval. At locations where the water depth is <104 m the bottom grid cell is not included in the euphotic zone. See Table 2 for a list of model parameter definitions and values.

[16] Remineralization of nitrate in the aphotic zone is parameterized as a first-order relaxation to observations with timescale τ:

$$\text{remineralization rate} = \frac{1}{\tau}\left[\mathrm{NO_3^*}(i,j,\sigma_\theta) - \mathrm{NO_3}\right],$$

where the reference nitrate concentration $\mathrm{NO_3^*}(i, j, \sigma_\theta)$ is interpolated from the modeled density using a three-dimensional lookup table, in which every (i, j) grid point has a reference nitrate-density relationship $\mathrm{NO_3^*}(i, j, \sigma_\theta^*)$ based on the nitrate field from *World Ocean Atlas* 1998, available on-line at http://www.nodc.noaa.gov/OC5/pr_woa.html [*Conkright et al.*, 1998] (hereinafter referred to as WOA98). The reference density field σ_θ^* is an average of the simulated density from the final 2 years of the spin-up period. Use of the model-derived density reference is necessary because of the slow drift of the simulated density away from the initial conditions during the integration.

[17] Density is a natural coordinate for referencing the nitrate field in this investigation, as the eddy-induced nutrient transport mechanism of interest here is a result of vertical isopycnal displacements. The underlying assumption of this model is that the nitrate-density relationship below the euphotic zone is restored on timescales comparable to or shorter than the interval between vertical displacements associated with the supply events. Let us examine this assumption by considering a fluid parcel caught in an upwelling event. As the parcel rises into the euphotic zone, nitrate is removed by photosynthesis. As the parcel is subsequently downwelled into the aphotic zone, it is refortified with nutrients. Thus it will bring new nitrate with it the next time it is upwelled. If the period of the vertical displacements was fast compared to the timescale for restoring the nitrate-density relationship, such a model would tend to over-predict the upward flux of nutrients.

Table 3. Estimated Timescale τ for Restoring the Nutrient-Density Relationship as a Function of Lateral Diffusivity K_H

K_H, m^2 s^{-1}	τ, days
1000	29
500	58
100	289
50	578
10	2894

However, this does not appear to be the case. Because the bulk of the nutrient transport associated with mesoscale eddies is associated with upwelling in their interiors during eddy formation and intensification, the timescale most relevant to such nutrient injections is that of an eddy lifetime [*McGillicuddy and Robinson*, 1997]. Typical mid-ocean eddies last for 6 months, with some Lagrangian drifter observations suggesting persistence of individual features for up to 430 days (see the review by *Richardson* [1993]). Given that an upwelled fluid parcel will be, statistically speaking, downwelled in the next dynamical event in which it participates, it can be argued that the nominal period of vertical displacements is of the order of a year.

[18] Estimation of the timescale for restoring the nitrate-density relationship is difficult because the underlying processes are not well understood. Several investigators have computed remineralization rates from seasonal variations in biogeochemical tracers, such as apparent oxygen utilization [e.g., *Jenkins and Goldman*, 1985; *Sarmiento et al.*, 1990] and the combined inventories of oxygen, dissolved inorganic carbon, and nitrate [e.g., *Ono et al.*, 2001]. Generally speaking, these studies indicate that aphotic zone remineralization is, on an annual basis, roughly consistent with net community production within the euphotic zone. Typically, such calculations in the aphotic zone are made on the basis of mean seasonal variations that have been smoothed in some way to remove higher-frequency variations. They yield estimates of remineralization necessary to maintain the observed seasonal cycles under the assumption of steady state. Thus such assessments provide an upper bound (of the order of several months) on the timescale over which mesoscale perturbations to the nutrient distribution are restored.

[19] There are at least three mechanisms by which the nitrate-density relationship might be restored following an eddy-driven productivity event. First, the nitrate deficit on a previously illuminated density surface could be restored by the remineralization of sinking particulate material from above. Clearly, that sinking flux would not necessarily have originated from the eddy-upwelling event itself because most of that material will have either already sunk or perhaps been downwelled as the previously uplifted density surface subsided. Indeed, idealized numerical simulations with a nutrient-phytoplankton-zooplankton-detritus ecosystem model reveal significant spatial disconnect between nutrient uptake and export flux [*Lima et al.*, 2002]. Thus this mechanism would rely primarily on the ambient flux of sinking particles. An estimate of the timescale for particle sinking can be made from the sinking rate and the vertical length scale over which particle flux decreases in the upper ocean. *Martin et al.* [1987] suggest that the e-folding scale of particle flux just below the euphotic zone in the open ocean is typically 100 m. Characteristic sinking rates of 1–10 m d^{-1} and a vertical length scale of 100 m imply remineralization timescales between 10 and 100 days.

[20] Alternatively, mesoscale patches of nitrate deficit could be restored via isopycnal mixing processes. Estimates of lateral diffusivity (which we equate with isopycnal diffusivity for the purposes of this discussion) in the open ocean vary widely and appear to be highly scale dependent. In the analysis of the spread of a deliberately released tracer in the eastern North Atlantic, *Ledwell et al.* [1998] documented lateral diffusivities of 0.07 m^2 s^{-1} operating on scales of 0.1–1 km, 2 m^2 s^{-1} operating on scales of 1–10 km, and of the order of 1000 m^2 s^{-1} operating on scales of 30–300 km. These estimates are roughly consistent with the scale dependence documented by *Okubo* [1971]. A recent review of diffusivity estimates on basin-scales in the North Atlantic by *Robbins et al.* [2000, Table 1] reports values generally of the order of 1000 m^2 s^{-1}, essentially equivalent to *Ledwell et al.* 's [1998] estimate for the largest scales resolved in their study. A restoring timescale τ for this process can be estimated using $\tau \sim L^2/K_H$, where K_H is the lateral diffusivity and L is a length scale. With an eddy radius of 50 km, the timescale for restoring mesoscale perturbations in the nutrient distribution vary widely with the diffusivity (Table 3). The use of the highest values of K_H represents an extreme upper bound; the eddies themselves are likely to be responsible for mixing at such large scales [e.g., *McWilliams et al.*, 1983]. Values in the range of 50–500 m^2 s^{-1} are probably more appropriate, yielding timescales that range from 2 months to 2 years. If the timescale for this process is 2 years, it becomes irrelevant. In contrast, a timescale of 2 months would not only be sufficient for restoring perturbations but would also constitute a pathway for additional nutrient supply during an isopycnal uplifting event.

[21] Finally, diapycnal processes can potentially contribute to restoration of the nutrient-density relationship, albeit on long timescales. Microstructure measurements and tracer release experiments suggest slow rates of mixing in the pycnocline of the order of 10^{-5} m^2 s^{-1} [e.g., *Lewis et al.*, 1986; *Gregg*, 1987; *Ledwell et al.*, 1993, 1998]. Results from surface layer tracer release experiments range from values close to that of the main thermocline (IronEx I, 2.5×10^{-5} m^2 s^{-1} [*Law et al.*, 1998]) to an order of magnitude larger than that of the main thermocline (GasEx98, 1.0×10^{-4} m^2 s^{-1} [*Zhang et al.*, 2001]; UK Prime, 1.95×10^{-4} m^2 s^{-1} [*Law et al.*, 2001]). This range of diffusivities implies a timescale of the order of 10^2–10^3 days for new nitrate to penetrate vertically over a 50-m interval of nutrient depletion, created by an eddy-driven nutrient injection event. Clearly, this latter estimate is longer than the yearly interval during which wintertime convection can temporarily mix down below the depth of the deepest isopycnals that can be illuminated in a subsequent eddy-upwelling event. Thus in regions where wintertime convection overshadows background vertical diffusion, the annual period sets an upper limit to the timescale on which diapycnal processes become relevant to this problem. In

Table 4. Runs

Run	Identifier	Duration	μ_0, mmol N m^{-3} d^{-1}	τ, days	Skill *S*, Nondimensional
1	13e	1992–1997	0.5	10	0.586
2	13e18	1992–1995	0.5	30	0.594
3	13e22a	1992–1995	0.5	60	0.610
4	13e22b	1992–1995	0.25	30	0.643

more permanently stratified areas the timescale could be considerably longer.

[22] In summary, these three mechanisms offer a wide variety of timescales for replenishment of nutrient-depleted isopycnals, which range from as short as 10 days to as long as a year. Given this uncertainty, which stems from a lack of understanding of the processes at work, the best strategy, from a modeling point of view, is to carry out sensitivity analyses of the results with respect to variations of the nutrient-restoring parameter. This will be discussed further in sections 2.4 and 3.1.

2.3. Advection Numerics

[23] The technical details of advection require special attention for biologically reactive tracers owing to two characteristics which can sometimes set them apart from typical physical tracers. First, biological tracers often vary by orders of magnitude over short spatial scales, making regions of such high gradients prone to significant overshoot/undershoot (dispersion) problems associated with centered-time/centered-space algorithms. This issue can become particularly troublesome due to the positive definite nature of such tracers; even the slightest negative concentrations can cause numerical instability in the equations governing biological dynamics.

[24] A variety of different advection schemes have been used in recent intercomparison studies [*Hecht et al.*, 1998; *Shchepetkin and McWilliams*, 1998; *Hasumi and Suginohara*, 1999; *Griffies et al.*, 2000; *Lévy et al.*, 2001a]. *Oschlies and Garçon* [1999] compared two positive definite schemes for tracer advection in their basin-scale biogeochemical model: first-order upwind differencing (also used by *Sarmiento et al.* [1993]) and the multidimensional positive definite central differences (MPDCD) of *Lafore et al.* [1998]. Results of their biogeochemical model were sensitive to the numerical diffusion implicit in the upwind scheme. Such diffusion is significantly reduced in the MPDCD algorithm. On the basis of the *Oschlies and Garçon* [1999] results, we chose to use MPDCD. Basically, it is a standard centered difference advection scheme with a limit condition placed on the fluxes. The flux limitation ensures that advection cannot remove more scalar than is present at any given time step. This is accomplished by multiplying all fluxes going out of a cell by the factor $\min[1.0, VC/(\Delta t \Sigma F_i^{\text{out}} A_i)]$, where V is volume, C is concentration, Δt is the time step, F_i^{out} is an outward flux, and A_i is the area of a grid cell face. Thus the MPDCD scheme is a simple scaling factor applied to fluxes, which is only different from 1.0 if the fluxes drive the concentration negative. Fortunately, the additional computational cost of this procedure is minor ($\sim$10% of the total run time) and its implementation is straightforward.

2.4. Experimental Design

[25] The computational demands of the simulations described herein are substantial. A single year of simulation time requires $\sim$14,000 processor hours on a 256-processor IBM SP; therefore only a small number of runs are practical. The experimental design is to initialize the nutrient transport model at the end of the 11.5-year physical model spin-up period, forcing it with surface fluxes from 1992 forward (see section 2.1). In order to avoid contamination by initial transients the first year of the coupled model solution is discarded and the remaining years are analyzed. A total of four runs of this type have been completed to date, ranging from 4 to 6 years in duration (Table 4). The simulations are identical with respect to physical forcing; this suite of runs is designed to investigate the sensitivity of the results to the two primary parameters of the nutrient uptake model: the maximum new production rate μ_0 and the restoring timescale τ.

3. Results

3.1. Evaluation of the Simulations

[26] Extensive measurements at several sites throughout the basin provide a basis on which to evaluate the simulations (Table 5). Although it is difficult to measure annual new production directly, several techniques have been used to make estimates based on observations, including geochemical tracers, nitrate utilization, primary production together with an *f* ratio, chlorophyll together with a model for new production, and sediment traps. Despite the significant differences in the underlying assumptions and methodology used in these various approaches, they have been used to compute a mean and range of annual new production for each site. Generally speaking, simulated annual new production for all four runs falls within the range of values estimated from the observations (Figure 1).

[27] Nitrate measurements constitute another obvious metric for model evaluation. Because the modeled nitrate is restored to climatology below the euphotic zone, comparisons with observations are most meaningful in the euphotic zone where the nitrate field is more free to evolve. Simulated nitrate near the top and bottom of the euphotic zone generally falls within the envelope of observed values (Figure 2). There are some clear discrepancies, such as the systematic under-prediction of wintertime nitrate values near the surface at the Bermuda Atlantic Time Series site (BATS). However, given the simplicity of the biological model used here, it is not surprising that the simulation does not match the observations perfectly in all areas of the basin.

[28] A quantitative metric of simulation skill can be generated through explicit computation of the differences between observations and predictions of annual new production, nitrate at 97 m, and nitrate at 5 m. A variety of algorithms are possible: We chose to compute the sum of squared differences between the observed and predicted quantities, normalized by the square of the mean value

Table 5. Annual New Production in the North Atlantic[a]

Annual New Production			
Simulated	Observed	Method	Reference
		BATS, 32°N, 64°W	
	0.45 ± 0.10	O_2 utilization	*Jenkins and Wallace* [1992]
	0.42 ± 0.09		*Jenkins and Goldman* [1985]
	0.46 ± 0.09	O_2 production	*Jenkins and Goldman* [1985]
	0.39 ± 0.16		*Spitzer and Jenkins* [1989]
	0.51 ± 0.14		*Spitzer and Jenkins* [1989]
	0.56 ± 0.16	He flux gauge	*Jenkins* [1988a]
	0.47 ± 0.15		W. J. Jenkins (personal communication, 2003)
	0.70 ± 0.20		*Jenkins* [1998]
0.63 ± 0.04	0.39–0.70[b]		
		NABE, 47°N, 20°W	
	0.90 ± 0.30	*PP* and O_2 data	*Balkanski et al.* [1999]
	1.26 ± 0.63	*PP* and *f* ratio	*Behrenfeld and Falkowski* [1997]
			Buesseler [1998]
			Martin et al. [1993]
	0.82 ± 0.44	*PP* and *f* ratio	*Antoine et al.* [1996]
			Buesseler [1998]
			Martin et al. [1993]
	1.89 ± 0.63	SeaWiFS and model	*Laws et al.* [2000]
	0.69	seasonal chlorophyll and NO_3	*Campbell and Aarup* [1992]
	0.43	seasonal chlorophyll and NO_3	*Strass and Woods* [1991]
1.48 ± 0.03	0.43–1.89[b]		
		OWSI, 59°N, 19°W	
	0.90 ± 0.30	*PP* and O_2 data	*Balkanski et al.* [1999]
	0.80	April–Aug. NO_3 utilization	*Sambrotto et al.* [1993]
	1.92 ± 0.35	*PP* and *f* ratio	*Behrenfeld and Falkowski* [1997]
			Sambrotto et al. [1993]
			Fasham et al. [1993]
	0.79 ± 0.16	*PP* and *f* ratio	*Antoine et al.* [1996]
			Sambrotto et al. [1993]
			Fasham et al. [1993]
	1.89 ± 0.63	SeaWiFS and model	*Laws et al.* [2000]
	0.53	seasonal chlorophyll and NO_3	*Campbell and Aarup* [1992]
1.47 ± 0.02	0.53–1.92[b]		
		EUMELI, 21°N, 31°W	
	0.45 ± 0.15	*PP* and O_2 data	*Balkanski et al.* [1999]
	0.19 ± 0.06	*PP* and $\delta^{15}N$ uptake	*Morel* [1999]
	0.13 ± 0.04	*PP* and *f* ratio	*Behrenfeld and Falkowski* [1997]
			Morel [1999]
	0.16 ± 0.05	*PP* and *f* ratio	*Antoine et al.* [1996]
			Morel [1999]
	0.10	seasonal chlorophyll and NO_3	*Campbell and Aarup* [1992]
	0.02	sediment traps (120 m)	*Passow and Peinert* [1993]
0.10 ± 0.01	0.02–0.45[b]		

[a]Annual new production is in mol N m^{-2} yr^{-1}. Note that the standard deviation reported for the simulated values reflects interannual variability in yearly means.
[b]Range of observational estimates for this site.

observed at each site. This normalization ensures equal weighting of all three quantities at all four sites in the assessment of the simulation skill *S*, defined as

$$S = \left[\frac{1}{4}\sum_{\text{Site}=1}^{4}\frac{1}{3}\left(\frac{(\text{ANP}_{\text{obs}} - \text{ANP}_{\text{sim}})^2}{\text{ANP}_{\text{obs}}^2} + \frac{\sum_{n=1}^{N_{\text{obs}}}\left(\text{NO}_3^{97\text{m}}{}_{\text{obs}} - \text{NO}_3^{97\text{m}}{}_{\text{sim}}\right)^2}{\sum_{n=1}^{N_{\text{obs}}}\left(\text{NO}_3^{97\text{m}}{}_{\text{obs}}\right)^2} + \frac{\sum_{n=1}^{N_{\text{obs}}}\left(\text{NO}_3^{5\text{m}}{}_{\text{obs}} - \text{NO}_3^{5\text{m}}{}_{\text{sim}}\right)^2}{\sum_{n=1}^{N_{\text{obs}}}\left(\text{NO}_3^{5\text{m}}{}_{\text{obs}}\right)^2}\right)\right]^{\frac{1}{2}}.$$

Note that the estimated mean annual new production from each site (Table 5) is used in the leading term, whereas individual point measurements of nitrate are used in the remaining terms. Mesoscale processes complicate model/data comparisons in this context as the simulation does not mimic the exact timing of specific eddy events present in the observations. Model fields are therefore smoothed with a 24-point Gaussian filter prior to extraction of the point-wise results in order to average over the local mesoscale variability. Unfortunately, similar treatment of the observations is not possible due to inadequate data coverage; thus even a statistically "perfect" model would not achieve a score of zero because of the mesoscale signal in the data. However, the above metric will be at a

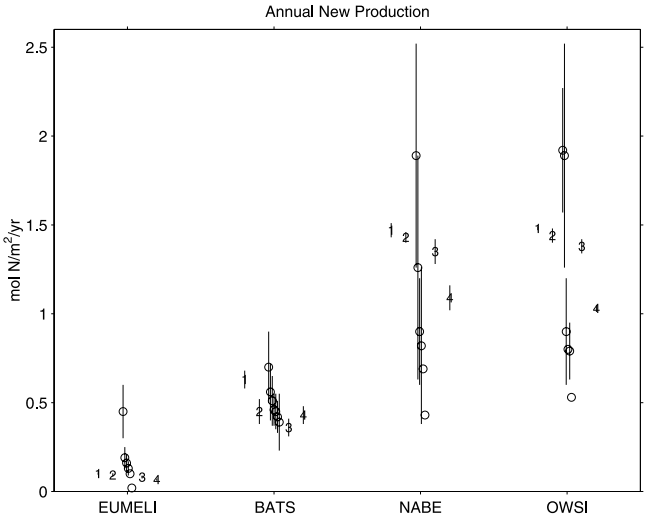

Figure 1. Simulated and observed annual new production at four sites in the North Atlantic. Observational estimates and associated uncertainties from Table 5 are indicated with open circles and error bars, respectively. Results from simulations 1–4 are shown as numerals; error bars associated with each run indicate the standard deviation associated with interannual variability. Prior to extraction of these point-wise results from the model, a 24-point *e*-folding scale Gaussian filter was applied to the solutions in order to ensure that the results are representative of regional averages. Model parameters for runs 1–4 are listed in Table 4.

minimum when the model's local background state matches that of the observations.

[29] On the basis of this metric, all four simulations provide roughly equivalent matches to observations, with values of *S* ranging from 0.59 to 0.64 (Table 4). Thus the results are not particularly sensitive to parameter variations within the range explored herein. Run 1 is the most skillful according to this metric, so it will be considered the "central" run, whose solution will be diagnosed in detail.

3.2. Mesoscale Phenomenology

[30] Mesoscale processes clearly impact new production throughout the basin (Figure 3; see also http://science.whoi.edu/users/mcgillic/pop-bgc/pop-bgc.html for an animated presentation of these results). This 10-day average of the simulated biological uptake term is replete with mesoscale structure in nearly all areas except for the subpolar region, where production is still light limited in early July.

[31] A zoomed-in view of the solution near the BATS site reveals the detailed relationships between the density field, nitrate, and new production (Figure 4). Energetic mesoscale features are present throughout the regional subdomain (Figure 4a). Eddy-driven enhancements of nitrate in the euphotic zone are clearly evident, most notably associated with positive density anomalies located at 32.5°N, 62.5°W; 34.5°N, 67.0°W; and 36.0°N, 62.0°W (Figure 4b). These areas are also hot spots of new production (Figure 4d). Although there is some enhancement of nitrate and new production associated with the frontal features between eddies, the strongest anomalies are in the interiors of the upwelling eddy features themselves. This phenomenology is consistent with regional model studies of *McGillicuddy and Robinson* [1997] and the conceptual model described in section 2.2.

[32] Note, however, that nitrate and new production in this snapshot are not enhanced in every eddy with a positive density anomaly (e.g., the strong feature at 29.0°N, 65.5°W). This results from a temporal aspect underlying the process of eddy-driven nutrient supply. Nutrient injections occur when eddies deflect nutrient-rich isopycnals upward into the euphotic zone, which happens during the formation and intensification phase of eddies with positive density anomalies in the upper ocean. As such features weaken, the isopycnals subside and net downwelling takes place in their interiors. This is exactly what is taking place in the eddy at 29.0°N, 65.5°W at the time of the snapshot shown in Figure 4: Even though it is still a strong feature (as indicated by the magnitude of the density anomaly), it is in the process of decay and is therefore no longer supplying nitrate to the euphotic zone. However, the signature of its prior impact on upper ocean productivity is clearly visible in the perturbation nutrient field (Figure 4c), which reflects the difference between the simulated nitrate and its reference value (based on the climatological relationship with density, to which the simulated nitrate is restored below the euphotic zone). The nitrate anomaly in the interior of this feature is a result of the biological uptake that occurred earlier in the eddy's lifetime, when those density surfaces were first upwelled. This temporal aspect of the eddy-driven upwelling process can be quite sporadic, owing to the synoptic-scale dynamics characteristic of densely populated eddy fields. Although the ultimate source of the eddies is baroclinic instability of the mean flow, eddy-eddy interactions tend to dominate the life cycles of individual features. These processes lead to complex relationships between synoptic physical, chemical, and biological fields.

3.3. Temporal Dynamics

[33] Time series of the balance of terms from spatially smoothed model results in selected areas reveal the relative contributions of the various transport terms fueling the simulated new production (Figure 5). Convection plays a significant role at the three northernmost sites. Both Ocean Weather Station India (OWSI) and the North Atlantic Bloom Experiment (NABE) site exhibit characteristics of the classical Sverdrup spring bloom: convective transport of nutrients into the surface layers during winter followed by their removal during springtime stratification. Convectively driven nutrient fluxes simulated at the two sites (Table 6) are in close agreement with climatological estimates made by *Williams et al.* [2000]. Latitudinal differences between these two sites are clearly evident: Convection occurs earlier and the bloom occurs later at OWSI than it does at NABE. At BATS, where an "entrainment bloom" occurs, the relationship between convection and new production is quite different [e.g., *Michaels et al.*, 1996; *Doney et al.*, 1996]. Nutrient input leads to a nearly simultaneous increase in new production because light is sufficient for rapid utilization. This type of bloom is characteristic of highly oligotrophic waters that are subject to wintertime convection. In contrast, convection plays no role in the permanently stratified waters at the Eutropic, Mesotrophic, and Oligotrophic (EUMELI)

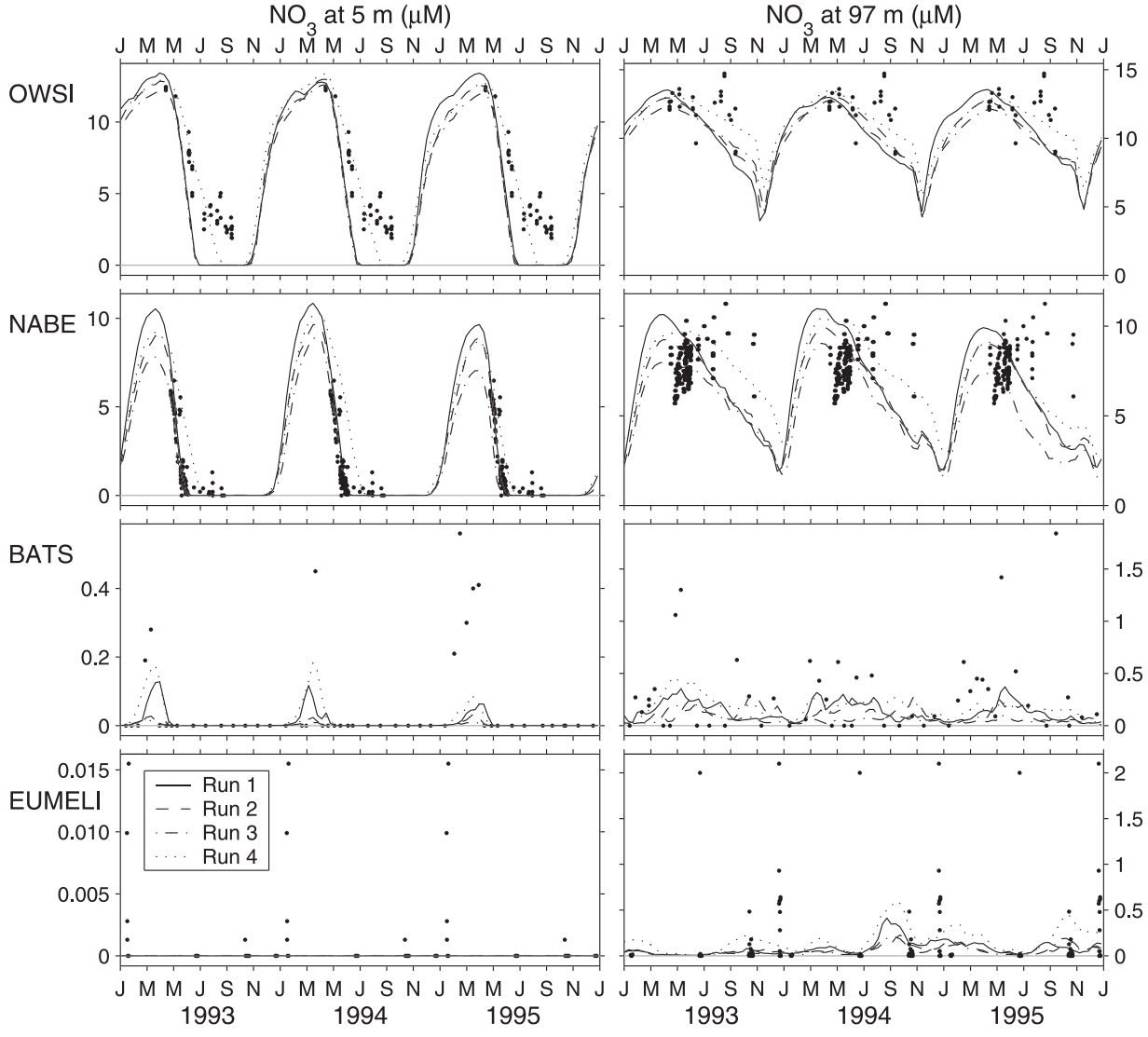

Figure 2. Simulated and observed nitrate at the top and bottom of the model euphotic zone (5 and 97 m, respectively) at four sites in the North Atlantic. Prior to extraction of these point-wise results from the model, a 24-point *e*-folding scale Gaussian filter was applied to the solutions. Observations at OWSI, NABE, and EUMELI are integrated into a composite year, which is repeated over the 3 years of simulation time shown here. Time series observations from 1993 to 1995 are used for comparison at BATS. Model parameters for simulations 1–4 are listed in Table 4.

site. Its simulated annual new production of 0.10 ± 0.01 is sustained by an equipartition of fluxes between vertical diffusion and vertical advection (Table 6). The vertical diffusive flux is always positive at EUMELI, and its temporal variations are slow; vertical advection fluctuates much more rapidly and is almost always positive. Horizontal advection does not yield a significant net contribution to the annual nutrient budget, although the term does reach relatively high values in association with intermittent pulses of eddy-driven vertical advection. A similar synchrony in episodes of horizontal and vertical advection is evident at the other sites as well. At OWSI and NABE, horizontal and vertical fluxes tend to balance each other, whereas at BATS, vertical advection is the dominant source of new production in summer.

3.4. Basin-Wide Term Balances

[34] The model solutions constitute a basis from which the various contributions to surface ocean productivity can be diagnosed. Integrated over the euphotic zone (Z_{EZ}), the time-averaged new production equation becomes

$$
\begin{aligned}
-\int_{Z_{EZ}}^{0} \overline{\mu \min(Q,L)}\,dz \;=\; & \int_{Z_{EZ}}^{0} \left(\frac{\partial}{\partial x}\left(\overline{u\mathrm{NO}_3}\right) + \frac{\partial}{\partial y}\left(\overline{v\mathrm{NO}_3}\right) \right) dz \\
& + \left(\overline{w\mathrm{NO}_3}\right)_{Z_{EZ}} \\
& - \int_{Z_{EZ}}^{0} K \left(\frac{\partial^4 \overline{\mathrm{NO}_3}}{\partial x^4} + \frac{\partial^4 \overline{\mathrm{NO}_3}}{\partial y^4} \right) dz \\
& + \left(\overline{M\mathrm{NO}_3}\right)_{Z_{EZ}},
\end{aligned}
$$

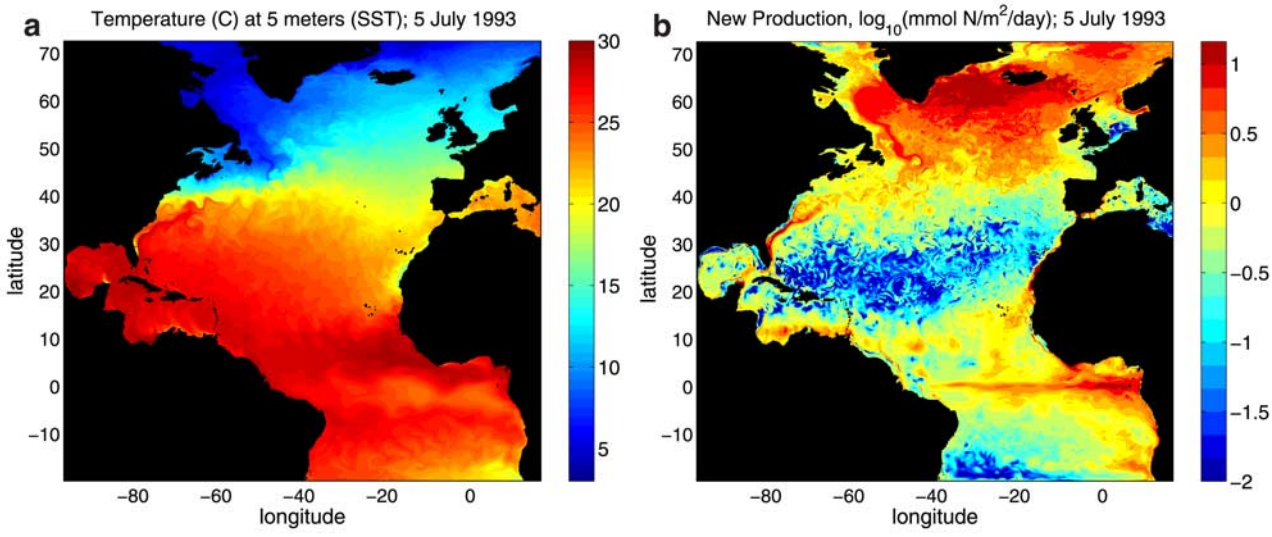

Figure 3. Snapshots of (a) temperature and (b) new production in a 0.1° simulation of the North Atlantic.

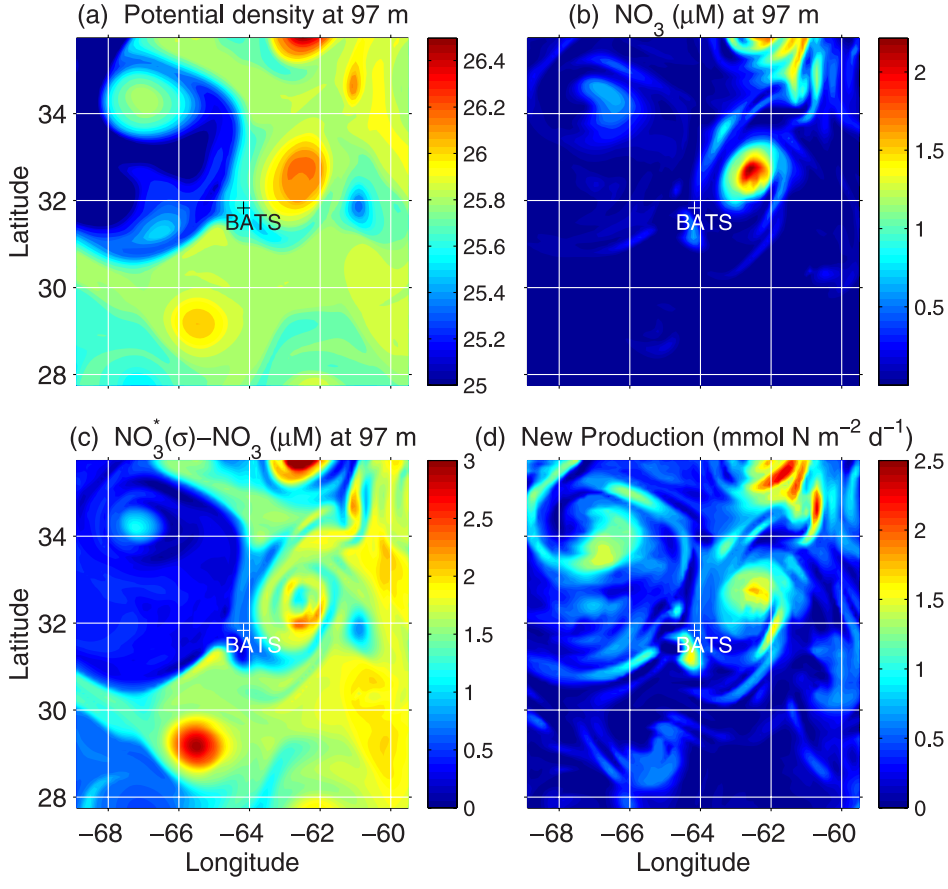

Figure 4. Snapshots of (a) potential density, (b) nitrate, (c) nitrate anomaly, and (d) new production extracted from Figure 3 in a subdomain of the Sargasso Sea. Nitrate anomaly is defined as the difference between simulated nitrate and the nitrate field computed from the simulated density field and the climatological nitrate-density relationship (to which the nitrate field is relaxed below the euphotic zone).

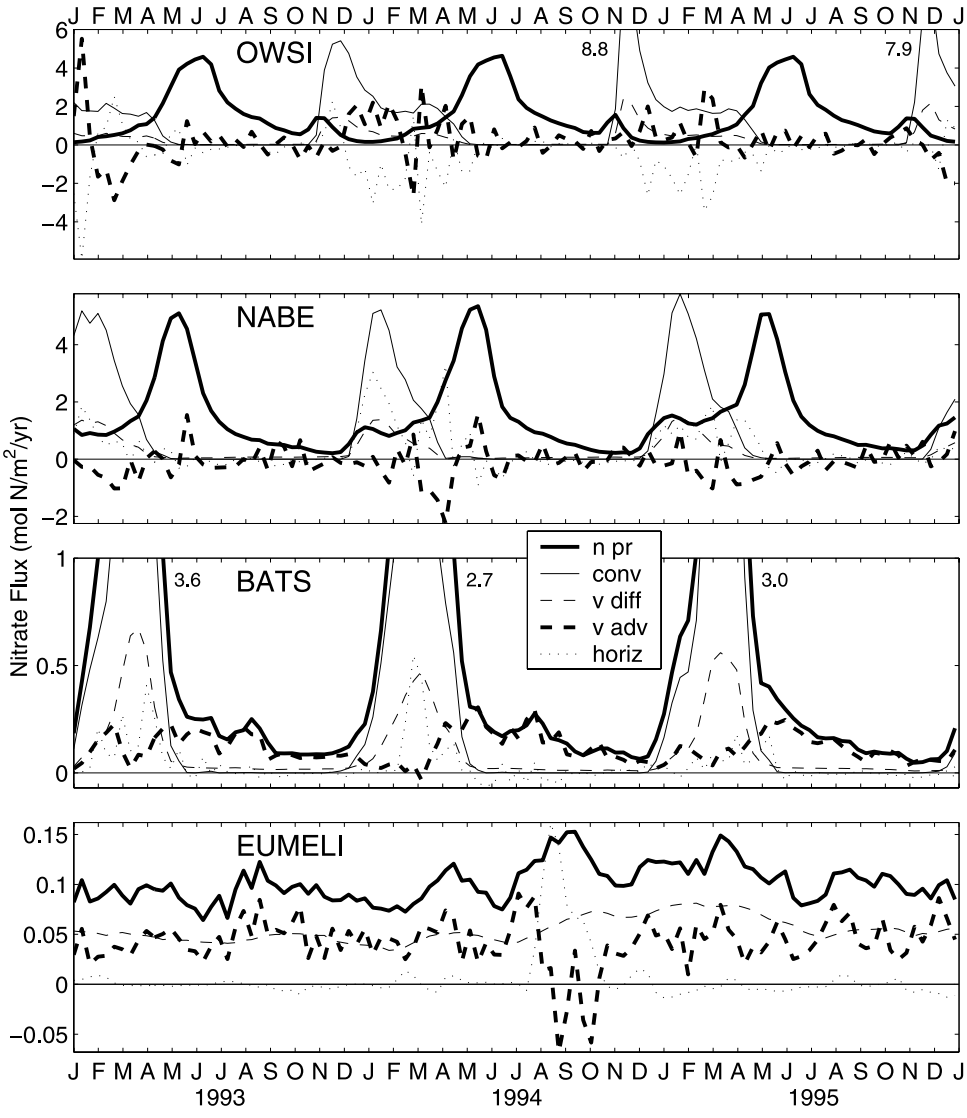

Figure 5. Term balances for nutrient cycling at selected sites throughout the basin (new production, bold solid line; convection, thin solid line; vertical diffusion, thin dashed line; vertical advection, bold dashed line; horizontal advection plus diffusion, dotted line). Prior to extraction of these point-wise results from the model, a 24-point *e*-folding scale Gaussian filter was applied to the solutions.

where u, v, and w are eastward, northward, and vertical velocities, respectively; over bars indicate temporal averaging. Aggregate vertical mixing terms $\left(\overline{M\mathrm{NO}_3}\right)_{Z_{EZ}}$ consist of a Richardson number formulation [*Pacanowski and Philander*, 1981], a background diffusivity of 10^{-5} m^2 s^{-1}, and a convective adjustment scheme. Horizontal mixing is scaled by the biharmonic coefficient K. Ten-day averages of each term above, in addition to all the state variables, are archived from the model solution, which facilitates separating the mean and eddying components of the advective terms. Eddy fluxes (indicated by prime symbols) are computed by differencing the time-averaged divergence of the advective flux (the "total" flux) and the divergence of the product of the time-averaged velocity and nitrate fields (the "mean" flux):

$$\frac{\partial}{\partial x}\left(\overline{u'\mathrm{NO}_3'}\right) = \frac{\partial}{\partial x}\left(\overline{u\mathrm{NO}_3}\right) - \frac{\partial}{\partial x}\left(\bar{u}\overline{\mathrm{NO}_3}\right)$$

$$\frac{\partial}{\partial y}\left(\overline{v'\mathrm{NO}_3'}\right) = \frac{\partial}{\partial y}\left(\overline{v\mathrm{NO}_3}\right) - \frac{\partial}{\partial y}\left(\bar{v}\overline{\mathrm{NO}_3}\right)$$

$$\left(\overline{w'\mathrm{NO}_3'}\right)_{Z_{EZ}} = \left(\overline{w\mathrm{NO}_3}\right)_{Z_{EZ}} - \left(\bar{w}\overline{\mathrm{NO}_3}\right)_{Z_{EZ}}.$$

Note that the so-called eddy fluxes include all time-dependent fluctuations in advection, which include seasonal variability as well as mesoscale dynamics.

[35] Maps of these various quantities reveal basin-scale heterogeneity in the balance of terms in the new production equation (Figure 6). The largest contributions to the simulated annual new production are vertical mixing, vertical advection, and horizontal advection. Horizontal mixing terms are several orders of magnitude smaller than the rest and are therefore not shown here.

Table 6. Simulated Nitrate Budgets and Annual New Production at Four Different Sites in the North Atlantic[a]

	BATS	NABE	OWSI	EUMELI
Horizontal transport[b]	0.04 ± 0.01	0.23 ± 0.07	−0.43 ± 0.19	0.00 ± 0.01
Advection	0.04 ± 0.01	0.23 ± 0.07	−0.43 ± 0.19	0.00 ± 0.01
Diffusion	0.00 ± 0.00	0.00 ± 0.00	0.00 ± 0.00	0.00 ± 0.00
Vertical mixing[c]	0.47 ± 0.04	1.32 ± 0.11	1.76 ± 0.12	0.05 ± 0.01
Convection	0.37 ± 0.03	1.02 ± 0.09	1.37 ± 0.09	0.00 ± 0.00
Diffusion	0.10 ± 0.01	0.30 ± 0.03	0.39 ± 0.03	0.05 ± 0.01
Vertical advection	0.12 ± 0.01	−0.09 ± 0.07	0.14 ± 0.17	0.05 ± 0.01
Annual new production	0.63 ± 0.04	1.48 ± 0.03	1.47 ± 0.02	0.10 ± 0.01

[a]Nitrate budgets and new production are in mol N m^{-2} yr^{-1}. Standard deviations are computed from yearly means and thus reflect interannual variability only.
[b]Horizontal transport is the sum of advection and diffusion.
[c]Vertical mixing is the sum of convection and diffusion.

[36] The spatial pattern of simulated annual new production is similar to that reported in prior studies [e.g., *Sarmiento et al.*, 1993]; that is, new production is generally higher in the subpolar and equatorial regions and lower in the subtropical gyre. Significant zonal asymmetry in the distribution of new production in midlatitudes is associated with the penetration of the western boundary current into the interior of the basin.

[37] High new production in the subpolar gyre (Figure 6a) is driven by the combination of vigorous vertical mixing (primarily due to winter convection (Figure 6b)) and mean upwelling that results from divergence of the wind-forced Ekman surface current (Figure 6d). Interestingly, the time-varying component of vertical advection is negative over a large portion of this region (Figure 6e), especially in areas where the maximum wintertime mixed layer depth exceeds 500 m (Figure 6b). In the southern flank of the gyre the magnitude of this sink is sufficient to overcome the mean upward vertical advection, causing the total vertical advection to be negative in that area (Figure 6c). In the northern part of the gyre, positive values in net vertical advection (Figure 6c) result from the dominance of mean upwelling (Figure 6d). Thus the dipole structure in total vertical advection (Figure 6c) arises from mean upwelling throughout the gyre (Figure 6d) and an eddy-driven downward flux in the southern portion (Figure 6e). Horizontal advection plays a significant role in this region as well. The large area of negative net lateral flux (Figure 6f) arises primarily from the contribution of mean horizontal advection (Figure 6g). Time-dependent horizontal advection in this area varies considerably on smaller scales but generally tends to reinforce the contribution of the mean. The cause of this negative lateral flux in the mean is clear upon examination of the mean velocity and nitrate fields (Figure 7): Northeastward advection by the North Atlantic current tends to import lower concentrations of nitrate into the subpolar gyre.

[38] The other large area of high new production is centered on the equator. It occupies a latitudinal band of ~20° in the western side of the basin and nearly double that on the eastern side. The vertical diffusive flux (Figure 6b) is enhanced throughout this region owing to the stronger vertical gradient in nitrate at the base of the euphotic zone. However, the main source of nutrients which fuel new production in this area is wind-driven upwelling, which is expressed in the mean field along the equator (Figure 6d) and in the time-dependent fluxes off the coast of Africa (Figure 6e). Eddy-driven vertical advection also tends to augment nitrate input throughout the rest of the region. Large lateral fluxes of nitrate (Figure 6f) are driven mostly by the mean field (Figure 6g). Eastward flow of the equatorial counter current across zonal gradients in the mean nitrate field causes a net sink of nitrate in the western two thirds of this latitude band (Figure 7). A net source of nitrate in the eastern third occurs where the countercurrent turns southeast and then south along the coast of Africa. Eddy-driven horizontal advection is negative all along the equator (Figure 6h) and thus tends to reinforce the mean flux in the west and counterbalance the mean flux in the east.

[39] The relatively modest new production characteristic of the subtropical gyre results from mean wind-driven downwelling and reduced vertical mixing, particularly in the southern portion (Figures 6d and 6b, respectively). Over most of the gyre, time-dependent vertical advection is positive (Figure 6c) and contributes a large fraction of the annual nutrient budget. This eddy-induced nutrient flux results from mesoscale dynamical processes such as those illustrated in Figure 4. Horizontal advection is close to zero over much of the subtropical gyre (Figures 6f–6h) owing to the lack of nitrate in the surface waters of this region. However, there is a significant input of nitrate due to horizontal advection along the northern edge of the gyre, particularly on the eastern side of the basin (Figure 6f). This lateral flux of nitrate into the gyre arises mostly from the mean fields (Figure 6g), into which the southward component of the North Atlantic drift delivers high nitrate water from the north (Figure 7).

4. Discussion

4.1. Diagnosis of Nitrate Budgets at Selected Sites

[40] How does this eddy-resolving simulation compare with the results from prior studies? Comparison with the coarse-resolution model of *Sarmiento et al.* [1993] and *Fasham et al.* [1993] (hereinafter referred to as FSSDW93) and the eddy-permitting model of *Oschlies et al.* [2000] (hereinafter referred to as OKG00) is made difficult by the fact that each uses a different physical model and biogeochemical formulation. Although nutrient

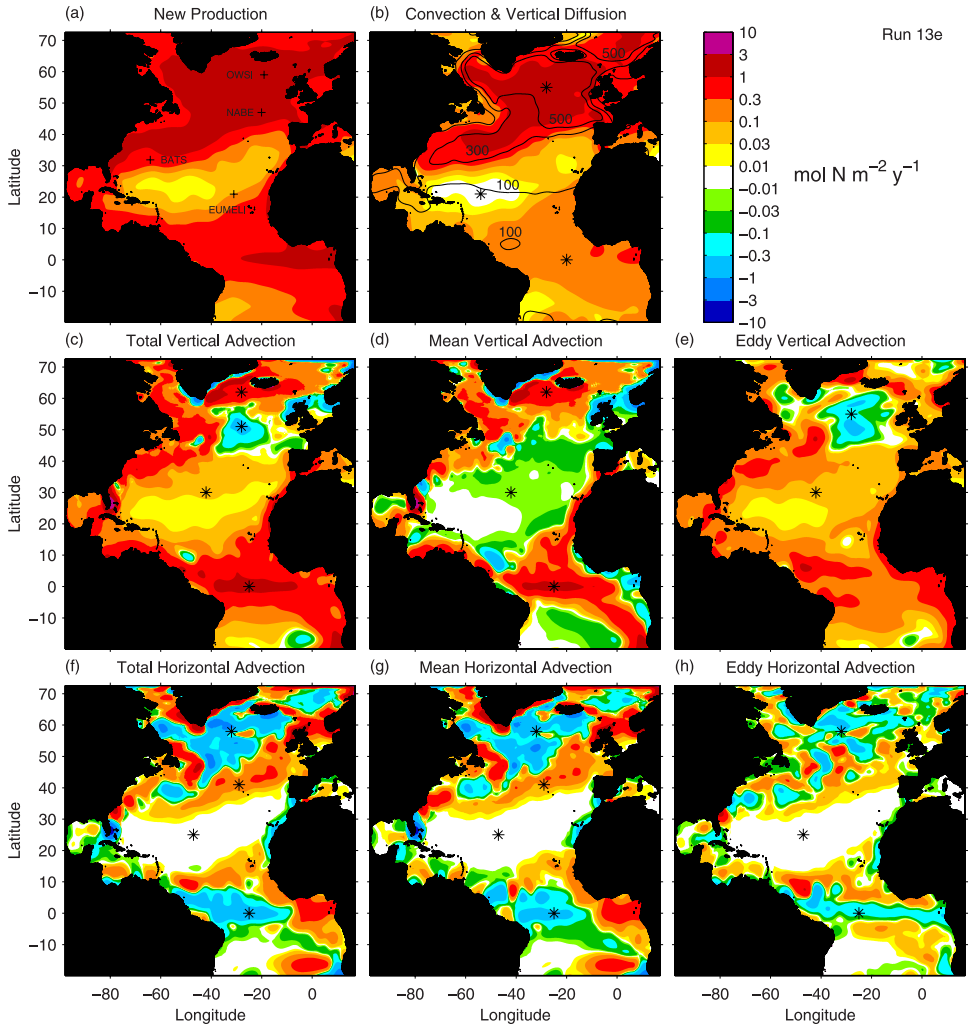

Figure 6. Dominant terms in the new production equation averaged over the euphotic zone for the period 1993–1997. Advective fluxes have been separated into their mean and eddying components (see text). All fields have been smoothed with a 24-point *e*-folding scale Gaussian filter. Asterisks indicate the main features of the solutions described in the text. Contours in Figure 6b indicate maximum wintertime mixed layer depths of 100, 300, and 500 m. Note that wintertime mixed layers inside the 500-m contour exceed that value by severalfold; additional contours are not shown for clarity of presentation.

supply to the upper ocean is a physically driven process, nutrient flux depends on the product of the nutrient fields and hydrodynamic transport. Therefore differences between models may reflect some convolution of these two constituents of the nutrient flux. An additional subtlety in model comparisons arises from the fact that smaller-scale motions that are explicitly included in high-resolution simulations may be represented in parameterized form in coarse-resolution models. For example, a flux divergence resulting from horizontal advection at fine resolution might appear (at least to some degree) as horizontal diffusion at coarse resolution. For all of these reasons, the following discussion of the similarities and differences between models will focus on general characteristics of the relative partitioning of horizontal and vertical processes in supplying nutrients to fuel new production. Indeed, integrated flux balances for the euphotic zone reveal quite distinct configurations in various sites throughout the North Atlantic (Figure 8).

4.1.1. Ocean Weather Station India (OWSI)

[41] Although the FSSDW93 coarse-resolution model and the eddy-resolving simulation predict quite different values of annual new production (0.44 versus 1.47 mol N m^{-2} yr^{-1}, respectively), the pathways of nutrient supply are in many ways similar in this region. Mean Ekman upwelling in the subpolar gyre, together with vertical mixing (both convection and diffusion), supply more nitrate than is consumed on an annual basis. This is compensated by a net sink due to horizontal transport, brought about by the advection of low-nitrate water into the region by the northeastward flowing branch of the North Atlantic Current. One important difference between the two cases pertains to the relative magnitude of vertical advection. In the coarse-resolution case, vertical advection is the largest nitrate source. In contrast,

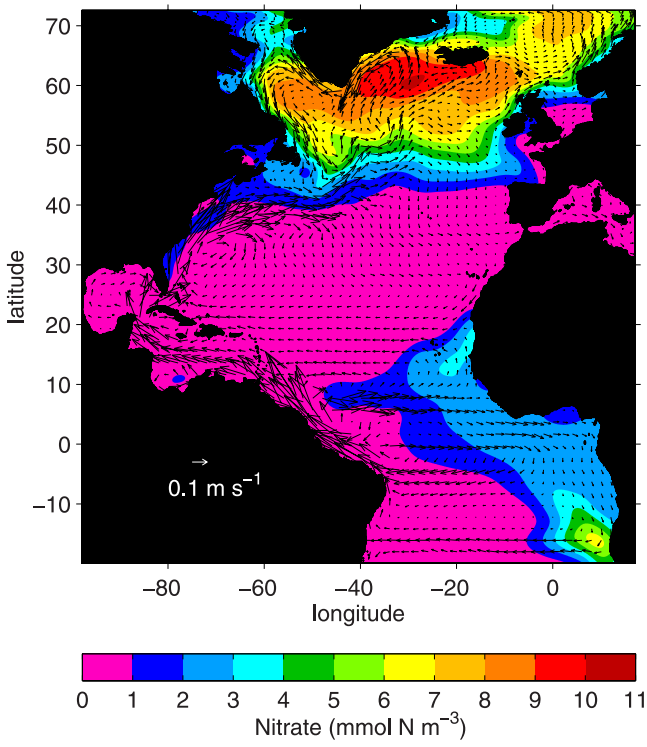

Figure 7. Mean nitrate (color shading) and velocity fields. Both quantities are averaged over the euphotic zone for the period 1993–1997 and then smoothed with a 24-point *e*-folding scale Gaussian filter.

mean Ekman upwelling of nutrients is somewhat muted in the eddy-resolving case. The latter is partially a result of the negative eddy fluxes in this region, which tend to counterbalance the mean wind-driven upwelling, an effect that is not evident in the coarse-resolution case.

4.1.2. North Atlantic Bloom Experiment (NABE)

[42] Similar to OWSI, the eddy-resolving model predicts a much larger annual new production than that simulated at coarser resolution: in this case 5 times higher than the eddy-permitting simulation of OKG00. More important, the relative contributions of the various fluxes are significantly different. Although both OKG00 and the present study suggest that vertical mixing is the largest source of nitrate at this site, the two models predict opposite impacts for horizontal advection. In OKG00, horizontal advection represents a net sink of nitrate that is 46% of annual new production, whereas the present study suggests that horizontal advection is a net source of nitrate, supplying 22% of the biological uptake. This discrepancy is likely due to the differing configurations of the North Atlantic Current in the two models. In the OKG00 model the North Atlantic Current tends to turn northward to the west of the Mid-Atlantic Ridge and flow west of Iceland [*Oschlies et al.*, 2000; *Oschlies and Willebrand*, 1996]. In the present model the North Atlantic Current penetrates much farther eastward, as observations indicate [*Smith et al.*, 2000]. At the NABE site a southward flowing branch tends to deliver high-nitrate water from the north, resulting in a net source from horizontal advection.

4.1.3. Bermuda Atlantic Time Series (BATS)

[43] All three models predict roughly the same annual new production at BATS, yet the mechanisms by which the nutrients are supplied are different in each case. The coarse-resolution simulations of FSSDW93 suggest that the primary source of nitrate is through horizontal advection. In the eddy-permitting case of OKG00 it is vertical mixing, with a smaller but still significant contribution from horizontal advection. Both FSSDW93 and OKG00 predict that vertical advection is a net sink of nitrate due to mean Ekman downwelling in the main subtropical gyre. In contrast, eddy-driven vertical fluxes in the present case are sufficient to overcome mean wind-forced downwelling to make vertical advection a net source of nitrate. Horizontal advection makes a small contribution, consistent with *Williams and Follows* [1998].

[44] How can these different views of the nitrogen cycle be reconciled? Although differences in the biogeochemical formulations of the three models cannot be dismissed, the fact that nitrate supply to the upper ocean is a physically driven process points toward more detailed scrutiny of the differences in physical frameworks used to drive the simulations. For example, the large horizontal flux of nitrogen into the Sargasso Sea in the FSSDW93 simulations is likely related to the impact of the horizontal mixing parameterization used at this relatively coarse resolution. In a careful analysis of the heat transport in GCMs, *Böning et al.* [1995] documented the presence of strong upwelling inshore of the Gulf Stream and lateral transport that significantly impact the structure of the simulated thermohaline circulation. The underlying causes of this aspect of the numerical solutions relate to the behavior of the mixing parameterization (which is typically applied on level surfaces in z coordinate models) in the presence of strongly sloping isopycnals, as in the western boundary current [*Veronis*, 1975]. This problem can be controlled to some degree by rotation of the mixing tensor to align with isopycnals [e.g., *Solomon*, 1971; *Redi*, 1982] and by increased resolution and a commensurate decrease in the coefficients of horizontal diffusion. This may explain the decreasing role of horizontal nitrate transport as the resolution is increased from 2° in FSSDW93, to 0.3° in OKG00, to 0.1° in the present case.

[45] Resolution of mesoscale processes is the other key factor controlling the nitrate budget at BATS. All three models capture the mean Ekman downwelling characteristic of this region. However, only in the present eddy-resolving case are mesoscale processes vigorous enough to overcome the mean downwelling. In terms of vertical advection the OKG00 eddy-permitting model is more similar to the FSSDW93 coarse-resolution model than the eddy-resolving case. The shift in vertical advection from a net sink of 0.13 mol N m^{-2} yr^{-1} in the OKG00 eddy-permitting simulation to a net source of 0.12 mol N m^{-2} yr^{-1} in the present study represents a swing of 0.25 mol N m^{-2} yr^{-1} in the nitrate budget: fully 40% of the annual new production.

4.1.4. Eutrophic, Mesotrophic, and Oligotrophic (EUMELI)

[46] Similarly striking differences are evident between the eddy-permitting and eddy-resolving simulations at the EUMELI site. Vertical advection supplies nearly half of the nitrate demand in the present study. In contrast, vertical

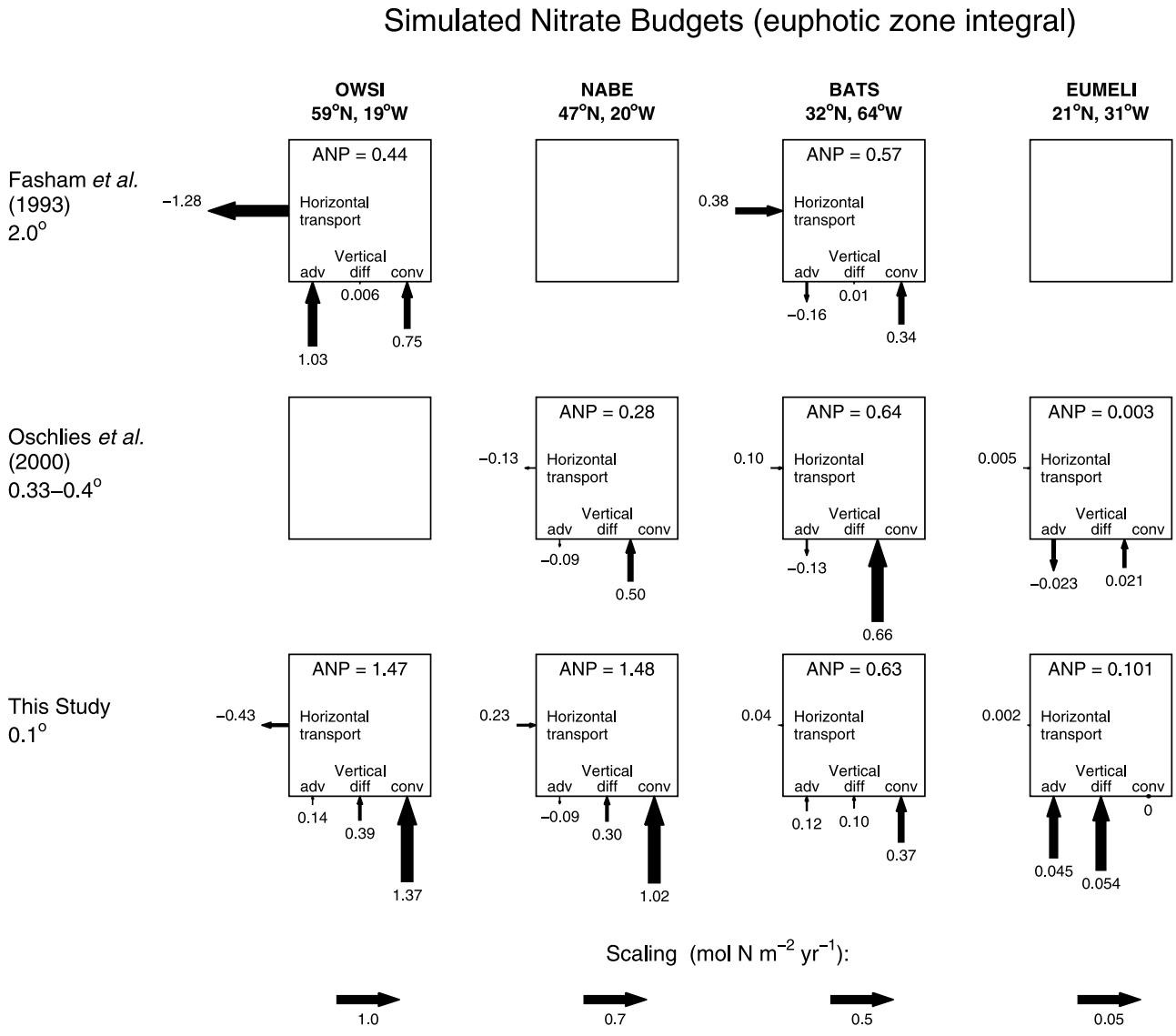

Figure 8. Comparison of simulated nitrate budgets (integrated over the euphotic zone) at four different sites in the North Atlantic. Prior to extraction of these point-wise results from the model, a 24-point *e*-folding scale Gaussian filter was applied to the solutions. Shown are results from (top) *Fasham et al.* [1993]; (middle) *Oschlies et al.* [2000]; and (bottom) this study. Flux diagrams are left blank in circumstances where values at that site were not reported in a given study. Note that the scales of the arrows used to depict flux magnitudes vary between sites in order to more clearly elucidate the differences between models.

advection is a net sink in the eddy-permitting case, with a magnitude more than 7 times larger than the simulated annual new production. Again, eddy-driven nutrient supply in the present case is able to overcome Ekman downwelling at this location. This effect, together with modestly enhanced vertical mixing, results in an annual new production more than 30 times larger in the present model than in the eddy-permitting case of OKG00.

4.2. Comparison With Another Eddy-Resolving Biogeochemical Simulation of the North Atlantic

[47] *Oschlies* [2002b] (hereinafter referred to as O02) reports on a simulation using a four-component ecosystem model (nutrients, phytoplankton, detritus, and zooplankton) embedded in a 2/15° × 1/9° resolution circulation model. Interestingly, the results are quite different from those presented herein, particularly with respect to the role of eddies in nutrient supply to the upper ocean. For example, basin-scale patterns in eddy-driven advection are quite different. Whereas the present model suggests time-dependent vertical advection is positive nearly everywhere throughout the tropics and subtropics, O02 predicts a strong band of negative eddy-driven vertical advection on the southeastern flank of the subtropical gyre. This feature is nearly collocated with a band of strong eddy-driven horizontal advection, thus suggesting an association with lateral

processes. Furthermore, it is aligned with a gradient in the spatially varying depth of the euphotic zone used in computation of the nutrient fluxes in the O02 results. It is not known whether the presence or absence of this feature is sensitive to the details of the flux diagnosis (i.e., a spatially varying euphotic zone in O02 versus a level surface in the present study).

[48] Detailed analysis of the term balances at the BATS site also reveals major differences. The simulated annual new production of 0.16 mol N m^{-2} yr^{-1} in the O02 study is fueled predominantly by wintertime convection (0.11 mol N m^{-2} yr^{-1}), with minor contributions from horizontal and vertical advection (0.03 and 0.02 mol N m^{-2} yr^{-1}, respectively). Much of the fourfold decrease in annual new production at the BATS site, from the eddy-permitting results of OKG00 to the O02 eddy-resolving case, can be attributed to reduction of nitrate input driven by wintertime convection (0.66 in OKG00 versus 0.11 mol N m^{-2} yr^{-1} in O02). This decrease in the convectively driven nitrate flux can, to some degree, be explained by differences in the forcing used in the OKG00 and O02 simulations. The former relied on climatological forcing, whereas the latter employed ECMWF products for the period 1989–1993. The 5-year period from 1989 to 1993 is characterized by relatively high values of the North Atlantic Oscillation index, during which wintertime convection near Bermuda tends to be shallower than normal [*Dickson et al.*, 1996].

[49] Why is the net flux due to vertical advection so much smaller in O02 than in the present study? The answer may be related to the way in which remineralization is represented in the two models: The present model relaxes to the observed nitrate-density relationship, whereas O02 computes remineralization explicitly in their prognostic ecosystem model. Interestingly, the O02 model under-predicts the observed correlation between nitrate and density in the 120- to 200-m-depth interval [O02, Figure 3d]. Because this is precisely the stratum from which waters are upwelled in eddy-induced nutrient supply events, it may explain why predictions of the flux due to vertical advection are smaller in O02 than they are in the present study. However, this may not be the sole cause of the apparent discrepancy. Other differences in the models, relating to both their hydrodynamic and biological formulations, may contribute as well.

4.3. What is the Nature of the Eddy-Driven Sink of Nutrients in the Subpolar Gyre?

[50] A curious aspect of the present model solutions is the significant downward transport of nutrients resulting from time-dependent processes in the subpolar gyre (Figure 6). This large area of negative vertical advection is not nearly so evident in a coarse-resolution implementation of the same model. Therefore the primary mechanism underlying this nutrient sink is likely to be associated with mesoscale processes. A time series of vertical transport terms at a site inside the nutrient sink in the high-resolution model reveals that it occurs primarily during the winter, in association with periods of deep convection (Figure 9). Correlations between fluctuations in vertical velocity and nutrient concentration result in an eddy-induced transport $\overline{w'NO_3'}$ sufficient to overcome advection by the mean vertical velocity $\left(\bar{w}\overline{NO_3}\right)$, which is upward due to Ekman suction in this region.

[51] The temporal lag of the eddy-induced sink with respect to the peak in convective activity suggests that the flux is associated with the mesoscale response to deep mixing. Indeed, mesoscale eddies have been shown to play a key role in restratification subsequent to deep convection [*Killworth*, 1976; *Madec et al.*, 1991; *Jones and Marshall*, 1993; *Visbeck et al.*, 1996, 1997; *Marshall*, 1997; *Khatiwala and Visbeck*, 2000] and more generally, subduction at upper ocean fronts [e.g., *Follows and Marshall*, 1994; *Spall*, 1995; *Nurser and Zhang*, 2000]. In fact, *Oschlies* [2002c] noted more realistic vernal shallowing of the mixed layer in a model of the North Atlantic as resolution was increased from eddy-permitting to eddy-resolving. The basic idea is that baroclinic instability tends to flatten isopycnals made upright by convective mixing. In an idealized model of a convective area of the ocean this results in an eddy-driven lateral flux of heat inward at the surface and outward at depth (Figure 10). Implied in this scenario is a downward eddy-driven flux in the interior of the convective area, which would not only tend to shallow the mixed layer but also to transport nutrients out of the euphotic zone. In this context the term "convective area" refers to the region over which convective activity takes place. Thus the convective area depicted in Figure 10 is not intended to represent an individual convective chimney but rather a large-scale density structure brought about by a collection of mesoscale and submesoscale convective events.

[52] Theoretical calculations provide a basis on which to estimate the downward flux of nutrients associated with this process. *Marshall* [1997] describes a cylindrically symmetric model of a convective region of the open ocean with characteristics similar to those which occur in the Labrador Sea [see *Marshall*, 1997, Figure 10]. Forced only by buoyancy loss at the surface, this model permits diagnosis of the eddy-induced circulations associated with geostrophic adjustment to the large-scale density gradients produced by convective activity. The model predicts a lateral heat flux inward near the surface to compensate for heat loss inside the area of deep convection. That flux is balanced by outwardly directed subduction along isopycnals in the deeper layers. Marshall's calculations suggest a subduction rate of the order of 1.5 sverdrup (Sv) across the 240-m-depth horizon. Partitioning that flux uniformly throughout his uppermost isopycnal layer, subduction across 104 m (the depth of the euphotic zone in the present model) would be approximately 0.6 Sv. Dividing this by the area of the convective region (200 km radius) yields an effective vertical velocity of 4.8×10^{-6} m s^{-1}. Applying this vertical velocity (w') to the perturbation nitrate concentration (NO_3') of 1 mmol m^{-3}(estimated from the standard deviation of wintertime nitrate values in the region) for a 3-month-long period of convection results in a net flux of -0.04 mol N m^{-2} yr^{-1}. This estimate is comparable to the eddy-driven sink of nutrients simulated in the Labrador Sea, where the flux generally falls between -0.03 and -0.1 mol N m^{-2} yr^{-1} (Figure 6e). The fact that this theoretical estimate so closely matches the numerical result supports the notion that mesoscale restratification processes are responsible for the eddy-induced nutrient sink simulated in the Labrador Sea. Note

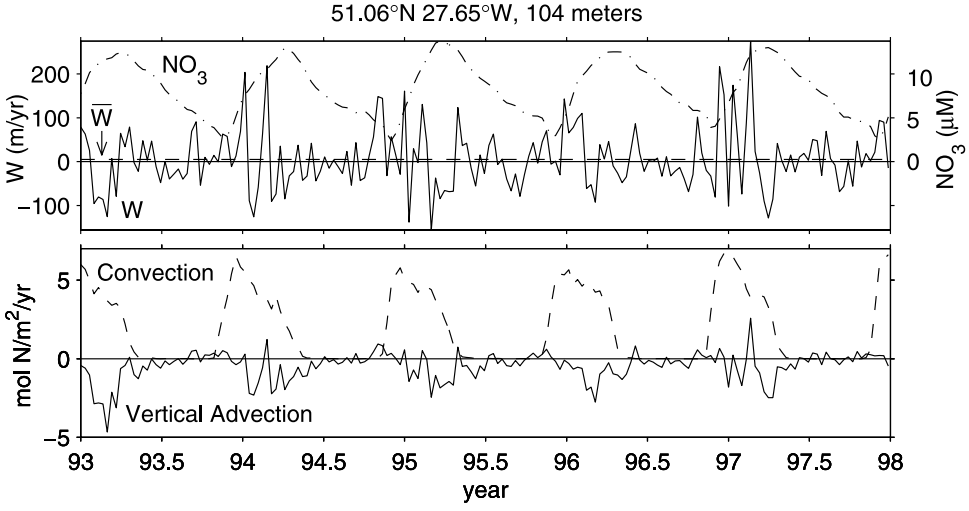

Figure 9. Time series of 10-day averages extracted from the model at 51.06°N, 27.65°W at 104 m. Prior to extraction of these point-wise results from the model, a 24-point *e*-folding scale Gaussian filter was applied to the solutions. In the top panel, vertical velocity is denoted by the solid line; mean vertical velocity is denoted by the dashed line; and nitrate concentration is denoted by the dash-dotted line. Note that the fluctuations in vertical velocity w are very much larger than the mean $\bar{w}$, which is upward in this region due to Ekman suction. In the bottom panel, nitrate fluxes due to vertical advection are denoted by the solid line; convection is denoted by the dashed line.

that much more extensive convection in the interior of the subpolar gyre leads to a stronger eddy-induced sink in that area (Figure 6e).

5. Conclusions

[53] Physical processes that transport nutrients into and out of the euphotic zone are essential regulators of the ocean's biological pump. In the last decade of research with three-dimensional basin-scale models it has become evident that nutrient transport in coupled physical-biogeochemical simulations is highly sensitive to the hydrodynamic fields on which such models are based. As spatial resolution is increased from coarse (∼2°) to eddy-permitting (∼0.3°) to eddy-resolving (∼0.1°), significant changes occur in the nutrient budgets with each increment. These changes consist not only of quantitative differences in nutrient fluxes but also of fundamental shifts in the processes controlling those fluxes.

[54] In the subtropics the eddy-resolving simulations described herein suggest that vertical advection by eddies is a primary pathway for nutrient supply. This finding is consistent with earlier regional studies [e.g., *McGillicuddy et al.*, 1998]. However, this effect does not appear to be captured in eddy-permitting models [*Oschlies and Garçon*, 1998; *Oschlies*, 2002a]. Interestingly, the eddy-resolving NPZD model results described by *Oschlies* [2002b] indicate a very modest eddy-driven nutrient supply in the subtropical gyre. The significant difference between the present results and those of *Oschlies* [2002b] is particularly striking given the similarity of the hydrodynamic simulations on which the coupled models are based. This suggests that the magnitude of the eddy-driven flux is sensitive to the nitrate concentrations at the base of the euphotic zone, which are largely controlled by remineralization. This process is implemented very differently in the two models. Remineralization is computed prognostically in the NPZD model in *Oschlies*'s [2002b] study: That approach turns out to yield correlations

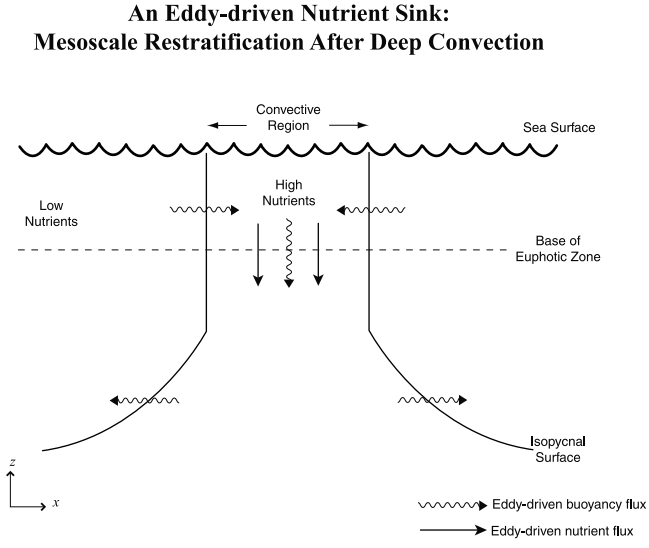

Figure 10. Schematic of the eddy-driven processes that tend to restratify an area of deep convection in the open ocean. Inward flux near the surface and outward flux at depth imply a downward eddy-driven transport that removes nutrients from the euphotic zone. Note that the convective area does not represent an individual chimney but the larger region over which mesoscale and submesoscale convective events take place.

between nitrate and density that are less than observed just below the euphotic zone. In contrast, the present model restores nitrate to climatology as a function of density and therefore preserves the observed correlations. Clearly, the issue of how to handle remineralization in such models is an important avenue for future research.

[55] In the subpolar gyre, vertical advection by eddies constitutes a sink of nutrients in the eddy-resolving simulations presented herein. A similar feature is evident in the results of *Oschlies* [2002b], suggesting that this result is not model dependent. Diagnosis of the model results indicates that the downward nutrient flux results from mesoscale processes associated with restratification following deep convection. The magnitude of the sink appears to be consistent with that estimated from *Marshall*'s [1997] kinematic model of eddy-driven transport applied to deep convection in the North Atlantic. In some ways this eddy-driven sink of nutrients is related to the mechanism described by *Lévy et al.* [1998, 1999], in which mesoscale restratification increases productivity following convection by releasing phytoplankton from light limitation. What we have described here is the counterpart to that process deeper in the water column: The same mesoscale dynamics that restratify the near-surface region pump nutrients out of the base of the euphotic zone. This flux occurs at a time when the ambient nutrients are well in excess of limiting concentrations, so the influence on productivity is not felt immediately. However, the impact on the nutrient budgets is significant and does lead to decreased productivity on seasonal timescales. Whether this process effects a quasi-permanent subduction of nutrients depends on the degree to which the downward flux penetrates beyond the depth of wintertime convection. It is not possible to make such a diagnosis in the present model given that nutrients are relaxed to climatology in the deep ocean. This is another important topic that will be addressed in future research.

[56] It has only recently become computationally feasible to conduct eddy-resolving biogeochemical simulations for entire ocean basins. Initial results from this and other studies reveal that mesoscale dynamics can have significant impacts on biogeochemical fluxes. It may be that even higher resolution will be necessary to capture all of the relevant dynamics; regional simulations suggest that frontal processes and submesoscale physics can play an important role in controlling production and subduction of phytoplankton in the upper ocean [*Mahadevan and Archer*, 2000; *Lévy et al.*, 2001b]. As large-scale, high-resolution simulations become more commonplace and higher-resolution data are collected, it will be possible to achieve a more thorough understanding of the mechanisms by which geophysical turbulence influences ocean biogeochemistry. Only then will it be possible to design and evaluate effective parameterizations for inclusion of these effects into global scale models. At present it appears that any such parameterizations would need to represent both sources (in the subtropics) and sinks (in the subpolar regions) of nutrients driven by mesoscale processes.

[57] **Acknowledgments.** We gratefully acknowledge the support of NSF, NASA, DOE, and JPL. The computations described herein were conducted using supercomputers at Los Alamos National Laboratory and the National Center for Atmospheric Research; we greatly appreciate our being granted access to those resources. We thank Frank Bryan and Michael Spall for fruitful discussions pertaining to this work. This is WHOI contribution 10698 and U.S. JGOFS contribution 815.

References

Antoine, D., J.-M. André, and A. Morel, Oceanic primary production, 2, Estimation at global scale from satellite (Coastal Zone Color Scanner) chlorophyll, *Global Biogeochem. Cycles*, *10*, 57–70, 1996.

Armstrong, R., J. Sarmiento, and R. Slater, Monitoring ocean productivity by assimilating satellite chlorophyll into ecosystem models, in *Ecological Time Series*, edited by T. M. Powell and J. H. Steele, pp. 371–390, Chapman and Hall, New York, 1995.

Balkanski, Y., P. Monfray, M. Battle, and M. Heimann, Ocean primary production derived from satellite data: An evaluation with atmospheric oxygen measurements, *Global Biogeochem. Cycles*, *13*, 257–271, 1999.

Barnier, B., L. Siefridt, and P. Marchesiello, Thermal forcing for a global ocean circulation model using a three-year climatology of ECMWF analyses, *J. Mar. Syst.*, *6*, 363–380, 1995.

Behrenfeld, M., and P. Falkowski, Photosynthetic rates derived from satellite-based chlorophyll concentration, *Limnol. Oceanogr.*, *42*, 1–20, 1997.

Böning, C., W. Holland, F. Bryan, G. Danabasoglu, and J. McWilliams, An overlooked problem in model simulation of the thermohaline circulation and heat transport in the Atlantic Ocean, *J. Clim.*, *8*, 515–523, 1995.

Browne, C. A., Liebig and the law of the minimum, in *Liebig and After Liebig: A Century of Progress in Agricultural Chemistry*, edited by F. R. Moulton, pp. 71–82, Am. Assoc. for the Adv. of Sci., Washington, D.C., 1942.

Bryan, K., A numerical method for the study of the circulation of the world ocean, *J. Comput. Phys.*, *4*, 347–376, 1969.

Buesseler, K., The decoupling of production and particulate export in the surface ocean, *Global Biogeochem. Cycles*, *12*, 297–310, 1998.

Campbell, J., and T. Aarup, New production in the North Atlantic derived from seasonal patterns of surface chlorophyll, *Deep Sea Res., Part A*, *39*, 1669–1694, 1992.

Capone, D., J. Zehr, H. Pearl, B. Bergman, and E. Carpenter, *Trichodesmium*: A globally significant marine cyanobacterium, *Science*, *276*, 1221–1229, 1997.

Chu, S., S. Elliot, and M. Maltrud, Global eddy permitting simulations of surface ocean nitrogen, iron, sulfur cycling, *Chemosphere*, *50*, 223–235, 2003.

Conkright, M. E., T. O'Brien, S. Levitus, T. P. Boyer, J. Antonov, and C. Stephens, *World Ocean Atlas 1998*, vol. 10, *Nutrients and Chlorophyll of the Atlantic Ocean*, *NOAA Atlas NESDIS 36*, 245 pp., Natl. Oceanic and Atmos. Admin., Silver Spring, Md., 1998.

Dadou, I., V. Garçon, V. Andersen, G. Flierl, and C. Davis, Impact of the North Equatorial Current meandering on a pelagic ecosystem: A modelling approach, *J. Mar. Res.*, *54*, 311–342, 1996.

Dickson, R., J. Lazier, J. Meincke, P. Rhines, and J. Swift, Long-term coordinated changes in the convective activity of the North Atlantic, *Prog. Oceanogr.*, *38*, 241–295, 1996.

Doney, S., D. Glover, and R. Najjar, A new coupled, one-dimensional biological-physical model for the upper ocean: Applications to the JGOFS Bermuda Atlantic Time Series (BATS) site, *Deep Sea Res., Part II*, *43*, 591–624, 1996.

Dutkiewicz, S., M. Follows, J. Marshall, and W. Gregg, Interannual variability of phytoplankton abundances in the North Atlantic, *Deep Sea Res., Part II*, *48*, 2323–2344, 2001.

Eppley, R., Temperature and phytoplankton growth in the sea, *Fish. Bull.*, *17*, 15–24, 1972.

Falkowski, P., D. Ziemann, Z. Kolber, and P. Bienfang, Role of eddy pumping in enhancing primary production in the ocean, *Nature*, *352*, 55–58, 1991.

Fasham, M., T. Platt, B. Irwin, and K. Jones, Factors affecting the spatial pattern of the deep chlorophyll maximum in the region of the Azores Front, *Prog. Oceanogr.*, *14*, 129–165, 1985.

Fasham, M., H. Ducklow, and S. McKelvie, A nitrogen-based model of plankton dynamics in the oceanic mixed layer, *J. Mar. Res.*, *48*, 591–639, 1990.

Fasham, M. J. R., J. L. Sarmiento, R. D. Slater, H. W. Ducklow, and R. Williams, Ecosystem behavior at Bermuda Station "S" and Ocean Weather Station "India": A general circulation model and observational analysis, *Global Biogeochem. Cycles*, *7*, 379–415, 1993.

Flierl, G., and C. Davis, Biological effects of Gulf Stream meandering, *J. Mar. Res.*, *51*, 529–560, 1993.

Follows, M., and J. Marshall, Eddy driven exchange at ocean fronts, *Ocean Modell. 102*, pp. 5–9, Hooke Inst. Oxford Univ., Oxford, England, 1994.

Franks, P. J. S., J. S. Wroblewski, and G. R. Flierl, Prediction of phytoplankton growth in response to the frictional decay of a warm-core ring, *J. Geophys. Res.*, *91*, 7603–7610, 1986.

Garçon, V., A. Oschlies, S. Doney, D. McGillicuddy, and J. Waniek, The role of mesoscale variability on plankton dynamics, *Deep Sea Res., Part II*, *48*, 2199–2226, 2001.

Gregg, M. C., Diapycnal mixing in the thermocline: A review, *J. Geophys. Res.*, *92*, 5249–5286, 1987.

Griffies, S., R. Pacanowski, and R. Hallberg, Spurious diapycnal mixing associated with advection in a z coordinate ocean model, *Mon. Weather Rev.*, *128*, 538–564, 2000.

Gruber, N., and J. L. Sarmiento, Global patterns of marine nitrogen fixation and denitrification, *Global Biogeochem. Cycles*, *11*, 235–266, 1997.

Hasumi, H., and N. Suginohara, Sensitivity of a global ocean circulation model to tracer advection schemes, *J. Phys. Oceanogr.*, *29*, 2730–2740, 1999.

Hecht, M. W., F. O. Bryan, and W. R. Holland, A consideration of tracer advection schemes in a primitive equation ocean model, *J. Geophys. Res.*, *103*, 3301–3321, 1998.

Hellerman, S., and M. Rosenstein, Normal monthly wind stress over the world ocean with error estimates, *J. Phys. Oceanogr.*, *13*, 1093–1104, 1983.

Hood, R. R., A. F. Michaels, and D. G. Capone, Answers sought to the enigma of marine nitrogen fixation, *Eos Trans. AGU*, *81*(13), 133, 138–139, 2000.

Hurlburt, H., and P. Hogan, Impact of 1/8° to 1/64° resolution on Gulf Stream model-data intercomparisons in basin-scale subtropical Atlantic Ocean models, *Dyn. Atmos. Oceans*, *32*, 283–329, 2000.

Hurtt, G., and R. Armstrong, A pelagic ecosystem model calibrated with BATS data, *Deep Sea Res., Part II*, *43*, 653–683, 1996.

Jenkins, W. J., Oxygen utilization rates in North Atlantic subtropical gyre and primary production in oligotrophic systems, *Nature*, *300*, 246–248, 1982.

Jenkins, W. J., Nitrate flux into the euphotic zone near Bermuda, *Nature*, *331*, 521–523, 1988a.

Jenkins, W. J., The use of anthropogenic tritium and helium-3 to study subtropical gyre ventilation and circulation, *Philos. Trans. R. Soc. London, Ser. A*, *325*, 43–61, 1988b.

Jenkins, W. J., Studying subtropical thermocline ventilation and circulation using tritium and ^{3}He, *J. Geophys. Res.*, *103*, 15,817–15,831, 1998.

Jenkins, W. J., and J. Goldman, Seasonal oxygen cycling and primary production in the Sargasso Sea, *J. Mar. Res.*, *43*, 465–491, 1985.

Jenkins, W. J., and D. Wallace, Tracer based inferences of new primary production in the sea, in *Primary Productivity and Biogeochemical Cycles in the Sea*, edited by P. Falkowski and A. Woodhead, pp. 299–316, Plenum, New York, 1992.

Jones, H., and J. Marshall, Convection with rotation in a neutral ocean: A study of ocean-deep convection, *J. Phys. Oceanogr.*, *23*, 1009–1039, 1993.

Khatiwala, S., and M. Visbeck, An estimate of the eddy-induced circulation in the Labrador Sea, *Geophys. Res. Lett.*, *27*, 2277–2280, 2000.

Killworth, P., The mixing and spreading phases of MEDOC I, *Prog. Oceanogr.*, *7*, 59–90, 1976.

Lafore, J.-P., et al., The meso-NH atmospheric simulation system, I, Adiabatic formulation and control simulations, *Ann. Geophys.*, *16*, 90–109, 1998.

Law, C., A. Watson, M. Liddicoat, and T. Stanton, Sulphur hexafluoride as a tracer of biogeochemical and physical processes in an open-ocean iron fertilization experiment, *Deep Sea Res., Part II*, *45*, 977–994, 1998.

Law, C., A. Martin, M. Liddicoat, A. Watson, K. Richards, and E. Woodward, A Lagrangian SF_6 tracer study of an anticyclonic eddy in the North Atlantic: Patch evolution, vertical mixing and nutrient supply to the mixed layer, *Deep Sea Res., Part II*, *48*, 705–724, 2001.

Laws, E., P. Falkowski, W. Smith, H. Ducklow, and J. McCarthy, Temperature effects on export production in the open ocean, *Global Biogeochem. Cycles*, *14*, 1231–1246, 2000.

Ledwell, J., A. Watson, and C. Law, Evidence for slow mixing across the pycnocline from an open-ocean tracer-release experiment, *Nature*, *364*, 701–703, 1993.

Ledwell, J. R., A. J. Watson, and C. S. Law, Mixing of a tracer in the pycnocline, *J. Geophys. Res.*, *103*, 21,499–21,529, 1998.

Levitus, S., Climatological atlas of the world ocean, *NOAA Prof. Pap. 13*, 173 pp., U.S. Govt. Print. Office, Washington, D.C., 1982.

Lévy, M., L. Memery, and G. Madec, The onset of a bloom after deep winter convection in the northwestern Mediterranean Sea: Mesoscale process study with a primitive equation model, *J. Mar. Syst.*, *16*, 7–21, 1998.

Lévy, M., L. Memery, and G. Madec, The onset of the spring bloom in the MEDOC area: Mesoscale spatial variability, *Deep Sea Res., Part I*, *46*, 1137–1160, 1999.

Lévy, M., A. Estublier, and G. Madec, Choice of an advection scheme for biogeochemical models, *Geophys. Res. Lett.*, *28*, 3725–3728, 2001a.

Lévy, M., P. Klein, and A. Treguier, Impact of sub-mesoscale physics on production and subduction of phytoplankton in an oligotrophic regime, *J. Mar. Res.*, *59*, 535–565, 2001b.

Lewis, M., W. Harrison, N. Oakley, D. Hebert, and T. Platt, Vertical nitrate fluxes in the oligotrophic ocean, *Science*, *234*, 870–873, 1986.

Lima, I. D., D. B. Olson, and S. C. Doney, Biological response to frontal dynamics and mesoscale variability in oligotrophic environments: Biological production and community structure, *J. Geophys. Res.*, *107*(C8), 3111, doi:10.1029/2000JC000393, 2002.

Lipschultz, F., and N. Owens, An assessment of nitrogen fixation as a source of nitrogen to the North Atlantic Ocean, *Biogeochemistry*, *35*, 261–274, 1996.

Madec, G., M. Chartier, P. Delecluse, and M. Crepon, A three-dimensional numerical study of deep-water formation in the northwestern Mediterranean Sea, *J. Phys. Oceanogr.*, *21*, 1349–1371, 1991.

Mahadevan, A., and D. Archer, Modeling the impact of fronts and mesoscale circulation on the nutrient supply and biogeochemistry of the upper ocean, *J. Geophys. Res.*, *105*, 1209–1225, 2000.

Marshall, D., Subduction of water masses in an eddying ocean, *J. Mar. Res.*, *55*, 201–222, 1997.

Martin, A. P., K. J. Richards, A. Bracco, and A. Provenzale, Patchy productivity in the open ocean, *Global Biogeochem. Cycles*, *16*(2), 1025, doi:10.1029/2001GB001449, 2002.

Martin, J., G. Knauer, D. Karl, and W. Broenkow, VERTEX: Carbon cycling in the northeast Pacific, *Deep Sea Res., Part A*, *34*, 267–285, 1987.

Martin, J., S. Fitzwater, R. Gordon, C. Hunter, and S. Tanner, Iron, primary production and carbon-nitrogen flux studies during the JGOFS North Atlantic Bloom Experiment, *Deep Sea Res., Part II*, *40*, 115–134, 1993.

McGillicuddy, D. J. Jr., and A. Robinson, Eddy induced nutrient supply and new production in the Sargasso Sea, *Deep Sea Res., Part I*, *44*, 1427–1449, 1997.

McGillicuddy, D. J. Jr., A. Robinson, D. Siegel, H. Jannasch, R. Johnson, T. Dickey, J. McNeil, A. Michaels, and A. Knap, Influence of mesoscale eddies on new production in the Sargasso Sea, *Nature*, *394*, 263–265, 1998.

McGillicuddy, D. J. Jr., R. Johnson, D. A. Siegel, A. F. Michaels, N. R. Bates, and A. H. Knap, Mesoscale variations of biogeochemical properties in the Sargasso Sea, *J. Geophys. Res.*, *104*, 13,381–13,394, 1999.

McGillicuddy, D. J. Jr., V. Kosnyrev, J. Ryan, and J. Yoder, Covariation of mesoscale ocean color and sea surface temperature patterns in the Sargasso Sea, *Deep Sea Res., Part II*, *48*, 1823–1836, 2001.

McNeil, J. D., H. W. Jannasch, T. D. Dickey, D. J. McGillicuddy Jr., M. A. Brzezinski, and C. M. Sakamoto, New chemical, bio-optical, and physical observations of upper ocean response to the passage of a mesoscale eddy off Bermuda, *J. Geophys. Res.*, *104*, 15,537–15,548, 1999.

McWilliams, J., et al., The local dynamics of eddies in the western North Atlantic, in *Eddies in Marine Science*, edited by A. Robinson, chap. 5, pp. 92–113, Springer-Verlag, New York, 1983.

Michaels, A., et al., sonal patterns of ocean biogeochemistry at the U.S. JGOFS Bermuda Atlantic Time-series Study site, *Deep Sea Res., Part I*, *41*, 1013–1038, 1994.

Michaels, A., D. Olson, J. Sarmiento, J. Ammerman, K. Fanning, R. Jahnke, A. Knap, F. Lipschultz, and J. Prospero, Inputs, losses and transformations of nitrogen and phosphorus in the pelagic North Atlantic Ocean, *Biogeochemistry*, *35*, 181–226, 1996.

Morel, F., Process studies in eutrophic, mesotrophic and oligotrophic regimes within the tropical northeast Atlantic, in *The Changing Ocean Carbon Cycle: A Midterm Synthesis of the Joint Global Ocean Flux Study*, *Int. Geosphere-Biosphere Programme Book Ser.*, vol. 5, edited by R. Hanson, H. Ducklow, and J. Field, pp. 338–374, Cambridge Univ. Press, New York, 1999.

Nurser, A. J., and J. W. Zhang, Eddy-induced mixed layer shallowing and mix layer/thermocline exchange, *J. Geophys. Res.*, *105*, 21,851–21,868, 2000.

Okubo, A., Oceanic diffusion diagrams, *Deep Sea Res. Oceanogr. Abstr.*, *18*, 789–802, 1971.

Ondercin, D. G., C. A. Atkinson, and D. A. Kiefer, The distribution of bioluminescence and chlorophyll during the late summer in the North Atlantic: Maps and a predictive model, *J. Geophys. Res.*, *100*, 6575–6590, 1995.

Ono, S., A. Ennyu, R. Najjar, and N. Bates, Shallow remineralization in the Sargasso Sea estimated from seasonal variations in oxygen and dissolved inorganic carbon and nitrate, *Deep Sea Res., Part II*, *48*, 1567–1582, 2001.

Oschlies, A., Nutrient supply to the surface waters of the North Atlantic: A model study, *J. Geophys. Res.*, *107*(C5), 3046, doi:10.1029/2000JC000275, 2002a.

Oschlies, A., Can eddies make ocean deserts bloom?, *Global Biogeochem. Cycles*, *16*(4), 1106, doi:10.1029/2001GB001830, 2002b.

Oschlies, A., Improved representation of upper-ocean dynamics and mixed layer depths of the North Atlantic on switching from eddy-permitting to eddy-resolving grid resolution, *J. Phys. Oceanogr.*, *32*, 2277–2298, 2002c.

Oschlies, A., and V. Garçon, Eddy-induced enhancement of primary production in a model of the North Atlantic Ocean, *Nature*, *394*, 266–269, 1998.

Oschlies, A., and V. Garçon, An eddy-permitting coupled physical-biological model of the North Atlantic, 1, Sensitivity to advection numerics and mixed layer physics, *Global Biogeochem. Cycles*, *13*, 135–160, 1999.

Oschlies, A., and J. Willebrand, Assimilation of Geosat altimeter data into an eddy-resolving primitive equation model of the North Atlantic Ocean, *J. Geophys. Res.*, *101*, 14,175–14,190, 1996.

Oschlies, A., W. Koeve, and V. Garçon, An eddy-permitting coupled physical-biological model of the North Atlantic, 2, Ecosystem dynamics and comparison with satellite and JGOFS local studies data, *Global Biogeochem. Cycles*, *14*, 499–523, 2000.

Pacanowski, R., and S. Philander, Parameterization of vertical mixing in numerical models of tropical oceans, *J. Phys. Oceanogr.*, *11*, 1443–1451, 1981.

Passow, U., and R. Peinert, The role of plankton in particle flux: Two case studies from the northeast Atlantic, *Deep Sea Res., Part II*, *40*, 573–585, 1993.

Platt, T., C. Gallegos, and W. Harrison, Photoinhibition of photosynthesis in natural assemblages of marine phytoplankton, *J. Mar. Res.*, *38*, 687–701, 1980.

Redi, M., Oceanic isopycnal mixing by coordinate rotation, *J. Phys. Oceanogr.*, *12*, 1154–1158, 1982.

Richardson, P., A census of eddies observed in North Atlantic SOFAR float data, *Prog. Oceanogr.*, *31*, 1–50, 1993.

Robbins, P., J. Price, W. Owens, and W. Jenkins, The importance of lateral diffusion for the ventilation of the lower thermocline in the subtropical North Atlantic, *J. Phys. Oceanogr.*, *30*, 67–89, 2000.

Sambrotto, R., J. Martin, W. Broenkow, C. Carlson, and S. Fitzwater, Nitrate utilization in surface waters of the Iceland Basin during spring and summer of 1989, *Deep Sea Res., Part II*, *40*, 441–457, 1993.

Sarmiento, J. L., G. Thiele, R. M. Key, and W. S. Moore, Oxygen and nitrate new production and remineralization in the North Atlantic subtropical gyre, *J. Geophys. Res.*, *95*, 18,303–18,315, 1990.

Sarmiento, J. L., R. D. Slater, M. J. R. Fasham, H. W. Ducklow, J. R. Toggweiler, and G. T. Evans, A seasonal three-dimensional ecosystem model of nitrogen cycling in the North Atlantic euphotic zone, *Global Biogeochem. Cycles*, *7*, 417–450, 1993.

Schulenberger, E., and J. Reid, The Pacific shallow oxygen maximum, deep chlorophyll maximum, and primary productivity: Reconsidered, *Deep Sea Res., Part A*, *28*, 901–919, 1981.

Shchepetkin, A., and J. McWilliams, Quasi-monotone advection schemes based on explicit locally adaptive dissipation, *Mon. Weather Rev.*, *126*, 1541–1580, 1998.

Siegel, D. A., D. J. McGillicuddy Jr., and E. A. Fields, Mesoscale eddies, satellite altimetry, and new production in the Sargasso Sea, *J. Geophys. Res.*, *104*, 13,359–13,379, 1999.

Slater, R., J. Sarmiento, and M. Fasham, Some parametric and structural simulations with a three-dimensional ecosystem model of nitrogen cycling in the North Atlantic euphotic zone, in *Towards a Model of Ocean Biogeochemical Processes*, edited by G. T. Evans and M. J. R. Fasham, pp. 261–294, Springer-Verlag, New York, 1993.

Smith, C., K. Richards, and M. Fasham, The impact of mesoscale eddies on plankton dynamics in the upper ocean, *Deep Sea Res., Part I*, *43*, 1807–1832, 1996.

Smith, R., J. Dukowicz, and R. Malone, Parallel ocean circulation modeling, *Physica D*, *60*, 38–61, 1992.

Smith, R., M. Maltrud, F. Bryan, and M. Hecht, Numerical simulation of the North Atlantic Ocean at 1/10°, *J. Phys. Oceanogr.*, *30*, 1532–1561, 2000.

Solomon, H., On the representation of isentropic mixing in ocean circulation models, *J. Phys. Oceanogr.*, *1*, 233–234, 1971.

Spall, M. A., Frontogenesis, subduction, and cross-front exchange at upper ocean fronts, *J. Geophys. Res.*, *100*, 2543–2557, 1995.

Spall, S., and K. Richards, A numerical model of mesoscale frontal instabilities and plankton dynamics, I, Model formulation and initial experiments, *Deep Sea Res., Part I*, *47*, 1261–1301, 2000.

Spitzer, W., and W. Jenkins, Rates of vertical mixing, gas exchange and new production: Estimates from seasonal gas cycles in the upper ocean near Bermuda, *J. Mar. Res.*, *47*, 169–196, 1989.

Strass, V., Chlorophyll patchiness caused by mesoscale upwelling at fronts, *Deep Sea Res., Part A*, *39*, 75–96, 1992.

Strass, V., and J. Woods, New production in the summer revealed by the meridional slope of the deep chlorophyll maximum, *Deep Sea Res., Part A*, *38*, 35–56, 1991.

Veronis, G., The role of models in tracer studies, in *Numerical Models of Ocean Circulation*, pp. 133–146, Natl. Acad. of Sci., Washington, D.C., 1975.

Visbeck, M., J. Marshall, and H. Jones, Dynamics of isolated convective regions in the ocean, *J. Phys. Oceanogr.*, *26*, 1721–1734, 1996.

Visbeck, M., J. Marshall, T. Haine, and M. Spall, Specification of eddy transfer coefficients in coarse-resolution ocean circulation models, *J. Phys. Oceanogr.*, *27*, 381–402, 1997.

Williams, R., and M. Follows, The Ekman transfer of nutrients and maintenance of new production over the North Atlantic, *Deep Sea Res., Part I*, *45*, 461–489, 1998.

Williams, R. G., A. J. McLaren, and M. J. Follows, Estimating the convective supply of nitrate and implied variability in export production over the North Atlantic, *Global Biogeochem. Cycles*, *14*, 1299–1313, 2000.

Woods, J., Mesoscale upwelling and primary production, in *Toward a Theory on Biological-Physical Interactions in the World Ocean*, edited by B. Rothschild, pp. 7–38, D. Reidel, Norwell, Mass., 1988.

Zhang, J.-Z., R. Wanninkhof, and K. Lee, Enhanced new production observed from the diurnal cycle of nitrate in an oligotrophic anticyclonic eddy, *Geophys. Res. Lett.*, *28*, 1579–1582, 2001.

L. A. Anderson and D. J. McGillicuddy Jr., Department of Applied Ocean Physics and Engineering, Woods Hole Oceanographic Institution, Bigelow 209b-MS 11, Woods Hole, MA 02543, USA. (landerson@whoi.edu; dmcgillicuddy@whoi.edu)

S. C. Doney, Department of Marine Chemistry and Geochemistry, Woods Hole Oceanographic Institution, Woods Hole, MA 02543, USA. (sdoney@whoi.edu)

M. E. Maltrud, Theoretical Fluid Dynamics, Los Alamos National Laboratory, T-3 MS B216, Los Alamos, NM 87545, USA. (maltrud@lanl.gov)